12

ULTRASONIC SHEAR VISCOMETER FOR LIQUID DROPLETS AND ITS APPLICATIONS

Edward Shalis

Technical Memorandum
File No. TM 77-207
April 25, 1977
Contract No. N00017-73-C-1418

Copy No. 9

The Pennsylvania State University
Institut for Science and Engineering
APPLIED RESEARCH LABORATORY
Post Office Box 30
State College, PA 16801

NAVY DEPARTMENT

NAVAL SEA SYSTEMS COMMAND

UNCLASSIFIED

SECURITY CLASSIFICATION OF THIS PAGE (When Data Entered)

REPORT DOCUMENTATION PAGE	READ INSTRUCTIONS BEFORE COMPLETING FORM
1. REPORT NUMBER: TM-77-207	2. GOVT ACCESSION NO. (9) Technical memo. for period and
4. TITLE (and Subtitle): ULTRASONIC SHEAR VISCOMETER FOR LIQUID DROPLETS AND ITS APPLICATIONS.	5. TYPE OF REPORT & PERIOD COVERED: PhD Thesis, August 1977
	6. PERFORMING ORG. REPORT NUMBER: TM-77-207 ✓
7. AUTHOR(s): Edward Shalis (10)	8. CONTRACT OR GRANT NUMBER(s): N00017-73-C-1418 (15)
9. PERFORMING ORGANIZATION NAME AND ADDRESS: The Pennsylvania State University, Applied Research Laboratory, P. O. Box 30, State College, PA 16801	10. PROGRAM ELEMENT, PROJECT, TASK AREA & WORK UNIT NUMBERS: (11) 25 Apr 77
11. CONTROLLING OFFICE NAME AND ADDRESS: Naval Sea Systems Command, Department of the Navy, Washington, D. C. 20362 (12) 86p.	12. REPORT DATE: April 25, 1977
	13. NUMBER OF PAGES: 84 pages & figures
14. MONITORING AGENCY NAME & ADDRESS (If different from Controlling Office): Office of Naval Research, Department of the Navy, Washington, D. C.	15. SECURITY CLASS. (of this report): Unclassified, Unlimited
	15a. DECLASSIFICATION/DOWNGRADING SCHEDULE

16. DISTRIBUTION STATEMENT (of this Report)

Approved for public release, distribution unlimited, per NSSC (Naval Sea Systems Command), 7/7/77

17. DISTRIBUTION STATEMENT (of the abstract entered in Block 20, if different from Report)

18. SUPPLEMENTARY NOTES

19. KEY WORDS (Continue on reverse side if necessary and identify by block number)

viscosity, viscometer, shear wave, ultrasonic, droplet, ultrasonic, droplet, liquid

20. ABSTRACT (Continue on reverse side if necessary and identify by block number)

An ultrasonic viscometer, capable of measuring small liquid volumes such as drops, was developed by utilizing the short effective path length of shear waves in liquids. The viscometer consists of an unplated quartz crystal excited to shear vibrations with the liquid drop to be tested placed on its surface. The vibrations of the natural modes of the quartz plate was represented by a mass-point compliant equation, and the viscosity equation was derived from the knowledge of the energy loss.

Suitable electronics was built to drive the crystal and to record the decaying

DD FORM 1 JAN 73 1473 EDITION OF 1 NOV 65 IS OBSOLETE

UNCLASSIFIED

20. ABSTRACT (continued)

vibrations. A crystal orientation analysis insured a dominant thickness-shear mode not coupled to flexure and face-shear motion. The amount of sound radiated was determined from the change in the quality factor when the crystal was vibrating alone in air and under vacuum.

Measurements were made on a variety of normal liquids and bonding agents over the frequency range from 200 to 1000 kHz, and the dynamic viscosity results scattered about the static value. A number of body fluids of man and domesticated animals were examined.

The response of the shear viscometer to changes in the rheological properties of bovine red blood cells was also measured. That is, the ability of red cells to deform was changed by hematological methods and the voscosity was measured before and after. It was found that the viscosity increased with the addition of sodium oleate, acetaldehyde, and hematocrit.

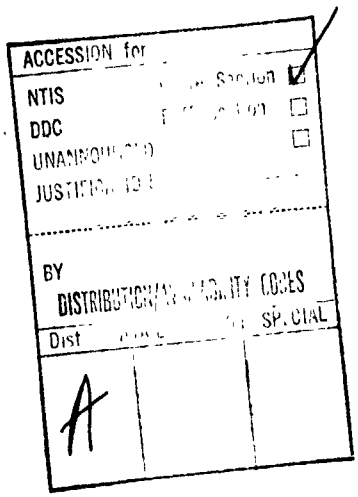

ACKNOWLEDGMENTS

The author would like to thank Professor Eugen J. Skudrzyk for suggesting the research problem and for his many helpful suggestions.

The author has profited from the many helpful discussions with Mitchell Belzar concerning the rheological properties of bovine red blood cells.

The author would like to thank Professor Rank for the financial support offered to him by the Physics Department of The Pennsylvania State University.

The author is especially grateful for all the encouragement given him by his sister Alvina, and her husband, Dr. Alan Lundberg.

This thesis was partially sponsored by ONR and supported by the Applied Research Laboratory of The Pennsylvania State University.

TABLE OF CONTENTS

TABLE OF CONTENTS (cont.)

LIST OF TABLES

LIST OF FIGURES

LIST OF FIGURES (cont.)

LIST OF SYMBOLS

c_{ij}	Elastic coeffici .
d_{mj}	Piezoelectric coefficients.
f	Friction force.
f_{x_f}	Frequency of flexure along x.
f_{x_s}	Frequency of face-shear along x.
f_{x_s}	Frequency of face-shear along z.
k	Wave number
k_ν	Wave number of ν^{th} mode.
v	Instantaneous velocity.
v_{sh}	Instantaneous shear velocity.
$\frac{\partial v}{\partial y}$	Velocity gradient.
x,y,z	System of rectangular coordinates.
x',y',z'	System of rotated rectangular coordinates.
A_n	Decay amplitude n ms after the start of the decay as seen on the oscilloscope screen.
D_i	Electric displacement component.
E	Total system energy.
E_i	Electric field component.
F	Force amplitude.
H	Hematocrit.
$H_\nu(A)$	Excitation constant for ν^{th} mode referred to the driving point (A).
K	Compliance.
K_ν^*	Effective compliance of the ν^{th} mode for a general excitation constant.

K_ν	Effective compliance of the ν^{th} mode for a unit excitation constant.
M	Mass.
M^Q	Crystal mass.
M_ν^*	Effective mode mass for a general excitation constant.
M_ν	Effective mode mass for a unit excitation constant.
M_ν^{sh}	Mode mass for shear vibrations.
M_ν^{dil}	Mode mass for dilatational vibrations.
Q	Quality factor.
R_ν^*	Effective mode resistance for a general excitation constant.
R_ν	Effective mode resistance for a unit excitation constant.
S_i	Strain component.
T_j	Stress component.
V_{sh}, V_0	Shear velocity amplitude.
V_{dil}	Dilatational velocity amplitude.
α	Absorption coefficient.
Δ	Ratio of dilatational to shear velocity.
$(1 + \Delta^2)^2$	Correction factor due to dilational motion.
δ	Decay constant.
η	Loss factor.
$\Delta\eta$	Change of system loss factor.
γ	Propagation distance.
λ_{sh}	Shear wavelength.
μ	Shear viscosity.
ξ	Instantaneous displacement in the x direction.

ξ_ν	Instantaneous displacement of the ν^{th} mode.
ξ_ν^0, ξ^0	Displacement amplitude.
$\langle \xi_\nu^2 \rangle$	Mean square value of the displacement for the ν^{th} mode.
ρ	Density.
ρ_L	Density of the liquid.
ρ_Q	Density of quartz.
σ_L	Contact area between the liquid and vibrator.
σ_Q	Surface area of quartz.
ω_ν	Angular frequency of ν^{th} mode.
ω_0	Resonance frequency.
ω_0^*	Effective resonance frequency of a point mass compliant element system.

CHAPTER I

INTRODUCTION

At the present time, experimental information dealing with the measurement of the viscosity of small liquid volumes, such as drops, is not available between 150 kHz and 5.0 MHz (1). Probably the first work done in this direction was performed by Skudrzyk and Dussik in the hospital at Ischl in 1947. A thin layer of the fluid found in the ventricle cavities of the human brain was placed over the surface of a quartz crystal that was excited to dilatational vibrations at its first three harmonic frequencies of 100 kHz. The fluid increased the damping of the crystal considerably and it seemed as if the large albumin chains in the fluid were responsible for the relaxation phenomenon in the frequency range from 100 to 500 kHz.

In 1968, Ghering (2) continued this work and investigated the energy losses in free and bonding liquids. The experimental data for films was puzzling: the magnitude of the energy losses were much greater than could be explained on the basis of longitudinal vibrations. The discrepancy was finally explained by the presence of shear motion in the quartz disc vibrator. Such motion usually leads to greater losses in free liquids. However, the energy dissipation for loaded films sandwiched between two transducers was still too great even when shear motion was accounted for.

Hosier (3) continued and extended the methodology using a shear vibrator. However, he encountered numerous difficulties that prevented the author from obtaining more detailed results. The range

of difficulties can best be illustrated by the following quote (4): ". . . the values of viscosity measured for water scattered between 0.5 centipoise to 450 centipoises. Similar results were obtained for glycerin where the viscosity ranged from 400 to 1100 centipoises whereas the static viscosity is approximately 600 centipoise."

1.1 Statement of the Problem

It is through these studies that a method to measure the viscosity of free liquids became possible. The task of this study was to eliminate the experimental errors of the previous authors and develop a high precision, inexpensive viscometer capable of measuring liquids of small volume, such as drops. This study utilizes the short effective path length of shear waves in liquids to examine drops. In liquids, shear waves are strongly attenuated and generate a boundary layer of motion in much the same way as electromagnetic waves generate the skin effect in metals, where an effective resistance similar to boundary viscosity exists. By analogy,

$$\gamma = \left(\frac{2\mu}{\omega\rho}\right)^{\frac{1}{2}} = \frac{1}{\alpha} \quad , \tag{1.1}$$

where γ is the skin depth defined as the propagation distance required for the amplitude of a shear wave to fall to $1/e$ of its initial value. In Equation (1.1)

μ = viscosity in poises,

ω = angular frequency in rad/sec,

ρ = density in gm/cm^3, and

α = absorption coefficient in cm^{-1}.

Table I illustrates the variation of the propagation distance γ, the shear wavelength λ_{sh}, and the shear velocity v_{sh}, for water over the frequency range from 0.2 to 1.0 MHz. Typically, in this frequency range, a shear wave is extinct after traveling a distance of 1.0 micron.

A method for measuring the viscosity of drops of liquids at high frequencies would have numerous practical applications. The standard method of measuring viscosity at the low physiological strain rates is to use a Brookfield Couette Viscometer which requires 500 milliliters of liquid. Equally significant, a thin layer of the test liquid does not slip along the rotating cylindrical wall and could possibly conceal the true viscosity if a mixture were measured.

At the present time, no viscometer is capable of measuring the viscosity of body fluids, such as those found in the joints, spinal column, and the ventricular cavities of the brain. A simple, direct measurement of their viscosity could be indicative of their state of health and diminish the need for existing operative techniques.

A droplet viscometer would be a new tool for examining other liquids of special interest to researchers in the medical fields. No viscometer is presently capable of measuring uncoagulated whole blood in less than four minutes. The shear viscometer makes it possible to measure the viscosity of fresh blood from a finger prick in less than one minute.

Medical schools are also interested in the effect that a change in the ability of red blood cells to deform has upon the viscosity of blood. The fluid nature of red blood cells and their incomplete

Table I. Shear parameters of water

F(kHz)	γ(cm)	$\alpha(cm^{-1})$	λ_{sh}(cm)	$v_{sh}\left(\frac{cm}{s}\right)$
235	1.16×10^{-4}	8.59×10^{3}	7.30×10^{-4}	172
283	1.06×10^{-4}	9.43×10^{3}	6.66×10^{-4}	188
402	0.88×10^{-4}	11.23×10^{3}	5.58×10^{-4}	224
503	0.80×10^{-4}	12.57×10^{3}	5.00×10^{-4}	251
1000	0.56×10^{-4}	17.70×10^{3}	3.54×10^{-4}	354

filling allows normal red cells to be deformed in a variety of shapes, ranging from a disk to a spheroid. Consequently, a deformed red cell will respond differently to a shear wave through the flow of the internal fluid of the cell and the bending of the outer membrane. This leads to changes in viscosity.

The study of erythrocytes is very pertinent as an application of the shear viscometer, since several authors have found the response of red blood cells to shear forces to be qualitatively similar to those of fluid drops in suspension (5).

1.2 Quartz Shear Viscometer

The shear viscometer consists of an unplated quartz crystal operating at the fundamental frequency and excited to shear vibrations by ultrasonic pulses. The unobstructed top surface is in contact with the liquid drop, and the bottom surface is returned to the hot side of the generator. After the power is shut off, the crystal becomes a receiver and converts the decaying vibrations into an electrical signal. These vibrations are amplified by a high gain, low leakage pulse

amplifier and displayed on a storage oscilloscope. The decay time of the vibration is determined from the oscilloscope curve.

Because of the great damping generated by the fluid, it was not necessary to design precision crystal holders to reduce interaction losses into the suspension. The quartz was simply placed on a flat metal base. The air cushion was sufficient to isolate its vibration from the base. The second electrode is a stiff metal plate located about 5.0 mm above the quartz surface, but not exactly parallel to it. Because of this separation and inclination, standing waves in the air gap were of no consequence to the vibration of the face of the crystal. On the other hand, this type of crystal holder confined sound radiation to the air spaces around the crystal and led to a quality factor of the order of 10^5 in air.

Because of the finite size of the quartz crystal, bending, torsion, shear and dilatational displacements are closely coupled and a quartz vibrator usually has many resonances close to the main mode of vibration (see Appendix A). Damping may then affect the main resonance differently from its neighbors and the vibration that appears in the decay may be very different from the one that had been excited by the generator.

The main problem here consists of finding a quartz crystal that has its resonance frequencies well separated from spurious frequencies so that the mode that dominates the decay is also the mode that generates the main resonance peak of the undamped crystal. It turns out that AT cut quartz bars made of certain dimensions (see Appendix B) lead to very satisfactory frequency response curves.

The shear viscometer is limited to the frequency range from 0.1 to 5.0 MHz. The lower range is controlled by the extreme thickness of the crystal, whereas the small amplitudes of vibrations are the limiting factor in the upper frequency. The viscometer is also restricted as to the amount of fluid that can be placed on its surface. Normally, a sample thickness of 2.0 to 5.0 mm is used. Increasing the liquid thickness beyond this range serves no purpose, since all the shear losses occur at the bottom of the layer within a distance of 1.0 micron. A thicker liquid will not increase the viscosity, since a 5.0 mm thickness already acts like an infinite medium.

CHAPTER II

THEORY OF THE SHEAR VIBRATOR

The vibration of an infinitely extended quartz surface (in the x direction) vibrating in the thickness-shear mode is described by the standing waves

$$\xi_\nu = \xi_\nu^0 \cos k\, y \quad , \tag{2.1}$$

where ξ_ν^0 is the constant amplitude and $k = n\pi/2b$. If the dimension along y is very great, standing shear waves along the y direction are also solutions. These modes are known as the zero-order uncoupled modes for infinitely extended surfaces. For vibrations of finite quartz plates, one shear mode cannot satisfy the boundary conditions at the side surfaces, and other modes of vibration exist and are coupled to each other, each one generating the other type of motion. The solution of a long quartz bar is always approximated by a sum of such zero-order mode functions (6) with different values of k,

$$\xi = \sum_{\nu=1}^{n} \xi_\nu^0 \cos k_\nu\, y \quad . \tag{2.2}$$

The superposition of the modes are spread out in a finite wave number range $k_1, \ldots, k_n$, and leads to a beat-like amplitude distribution in space,

$$\xi = \xi_0'(x) \cos k\, y \quad , \tag{2.3}$$

where $\xi_0'(x)$ is a slowly varying function of x, with a maximum value in

the center and smaller values at the ends. However, the exact velocity distribution $\xi'_{\ell}(x)$ for quartz surfaces of finite extent are unknown and must be found experimentally.

The vibration of the natural modes of a quartz plate can also be represented by an equation similar to that of a point mass vibrating with a resistance and compliance (7),

$$M^*_\nu \ddot{\xi}_\nu + R^*_\nu \dot{\xi}_\nu + \frac{1}{K^*_\nu} \xi_\nu = Fe^{j\omega t} \quad . \tag{2.4}$$

The quantities $M^*_\nu, R^*_\nu, K^*_\nu$ are the mode parameters and represent the effective mass, resistance, and compliance for a particular natural function ξ_ν, referred to the observation point A and the total driving force F. The mode parameters are given by

$$M^*_\nu(A) = \frac{M_\nu(A)}{H_\nu(A)} \quad ,$$

$$R^*_\nu(A) = \frac{\omega^2_\nu}{\omega} \eta M^*_\nu(A) \tag{2.5}$$

and

$$K^*_\nu(A) = \frac{1}{\omega^2_\nu M^*_\nu(A)} \quad ,$$

where $H_\nu(A)$ is the fraction of the total driving force that is available for exciting the ν^{th} mode, and is known as the excitation constant.

If the driving point coincides with the point of observation, $H_\nu = 1$ regardless of the complexity of the system (8), then the effective mode parameters become

$$M_\nu = \frac{\langle \xi_\nu^2 \rangle}{\xi_\nu^2(A)} M \quad ,$$

$$R_\nu = \frac{\omega_\nu^2}{\omega} \eta M_\nu \tag{2.6}$$

and

$$K_\nu = \frac{1}{\omega_\nu^2 M_\nu} \quad ,$$

where ξ_ν are the natural functions and ω_ν the corresponding natural frequencies.

In our case, the force is removed and the free vibrations decay with time because of internal friction. Experiments show that the decay is exponential when damping is not excessively large (9). Differentiating and rearranging terms, letting the natural mode now be expressed by ξ,

$$\frac{d^2}{dt^2}\dot{\xi} + 2\delta \frac{d}{dt}\dot{\xi} + \omega_\nu^2 \dot{\xi} = 0 \quad , \tag{2.7}$$

where

$$\delta = \frac{R_\nu}{2M_\nu} = \text{decay constant}$$

and

$$\omega_0 = \left(\frac{1}{M_\nu K_\nu}\right)^{\frac{1}{2}} = \text{resonance frequency} \quad .$$

A solution is given by

$$\dot{\xi} = \dot{\xi}_0 \, e^{\left(-\delta \pm \sqrt{\delta^2 - \omega_0^2}\right)t}$$

and

$$\dot{\xi} = \dot{\xi}_0 \, e^{\left(-\delta \pm j\omega_0^*\right)t} \quad , \tag{2.8}$$

where

$$\omega_0^* = \sqrt{\omega_0^2 - \delta^2} \tag{2.9}$$

and $\dot{\xi}$ has a periodic amplitude decay given by

$$\dot{\xi}_0 \, e^{-\delta t} = e^{-\frac{\omega_0 \eta}{2} t} \quad , \tag{2.10}$$

where δ is the decay constant of the envelope of the vibrations and ω_0^* is the effective resonant frequency of the point-mass element.

Assuming that the maximum displacement is equal to the displacement amplitude, we have

$$\dot{\xi} = \xi_0 (-\delta) e^{-\delta t} \quad . \tag{2.11}$$

The maximum elastic energy of the vibration,

$$E = \frac{1}{2} M_v \dot{\xi}^2 \tag{2.12}$$

is then given by

$$E = \frac{1}{2} M_v \delta^2 \xi_0^2 \, e^{-2\delta t} \quad , \tag{2.13}$$

The rate of energy lost per cycle $\frac{dE}{dt}$ is

$$\frac{dE}{dt} = - 2\delta E \tag{2.14}$$

and the decay then follows from

$$\delta = \frac{\frac{dE}{dt}}{2E} \quad . \tag{2.15}$$

The decay constant is therefore a function of the energy loss and the maximum vibrational energy of the crystal. Because of the strong coupling of the dilatational and shear modes due to the boundary conditions at the side surfaces, E represents the total elastic energy, consisting of shear and dilatational components, i.e.,

$$E = \frac{1}{2} M^{\nu}_{sh} V^2_{sh} + \frac{1}{2} M^{\nu}_{dil} V^2_{dil} \tag{2.16}$$

where V_{sh} and V_{dil} are the velocity amplitudes for shear and dilatation. Assuming $M^{\nu}_{sh} = M^{\nu}_{dil}$,

$$E = \frac{1}{2} M^{Q}_{\nu} V^2_{sh} (1 + \Delta^2) \quad , \tag{2.17}$$

where

$$\Delta = \frac{V_{dil}}{V_{sh}} \quad . \tag{2.18}$$

Let us consider the semi-infinite fluid layer ($y \geq 0$) which is excited to shear vibrations by the plane crystal surface at $y = 0$. The surface of the crystal moves in its plane sinusoidally with an amplitude $V_{sh} = V_0$ and a frequency ω. Using Newton's second law for the resultant stress on a layer of fluid yields the Stokes wave equation,

$$\rho \frac{\partial v}{\partial t} = - \mu \frac{\partial^2 v}{\partial y^2} \quad . \tag{2.19}$$

The velocity field for periodic waves is described by

$$v = V_0 e^{-k_0 y} e^{j(\omega t - k_0 y)} \quad , \tag{2.20}$$

where

$$k_0 = \left(\frac{\omega \rho}{2\mu}\right)^{\frac{1}{2}} \quad . \tag{2.21}$$

The reaction force exerted by the fluid due to this motion is given by,

$$f\Big|_{y=0} = - \sigma_L \mu \frac{\partial v}{\partial y}\Big|_{y=0}$$

$$= \mu k_0 V_0 \sigma_L (\cos \omega t - \sin \omega t) \quad , \tag{2.22}$$

and the power dissipated (that is, the work performed by the crystal surface on the viscous film) is

$$\frac{\partial E}{\partial t}\Big|_{y=0} = \lim_{T \to \infty} \frac{\sigma_L}{T} \int_0^T \mu k_0 V_0 (\cos \omega t - \sin \omega t) V_0 \cos \omega t \, dt$$

$$= \frac{1}{2} \mu k_0 \sigma_L V_0^2 \quad . \tag{2.23}$$

The decay constant thus becomes

$$\delta = \frac{\frac{dE}{dt}}{2E} \tag{2.24}$$

$$\delta = \frac{\frac{1}{2} \mu k_0 \sigma_L V_0^2}{2 \frac{1}{2} M_0 V_0^2 (1 + \Delta^2)}$$

and

$$\delta = \frac{\frac{1}{2}\mu k_0 \sigma_L}{M_\nu^Q(1 + \Delta^2)} \quad . \tag{2.25}$$

Since the increase of the decay constant for a crystal loaded by a drop of fluid is linearly proportional to the increased shear loss,

$$\frac{\omega}{2}\Delta\eta = \frac{\frac{1}{2}\mu\left(\frac{\omega\rho}{2\mu}\right)^{\frac{1}{2}}\sigma_L}{M_\nu^Q(1 + \Delta^2)} \tag{2.26}$$

and

$$\mu = \frac{2\omega}{\rho_L}\left(\frac{\Delta\eta}{\sigma_L}\right)^2\left(M_\nu^Q\right)^2 (1 + \Delta^2)^2 \quad . \tag{2.27}$$

The viscosity of a small volume of liquid depends on the change in system loss factor $\Delta\eta = \frac{2}{\omega(t_e^0 - t_e)}$, the liquid contact area σ_L, the crystal frequency ω, the liquid density ρ_L, the correction factor $(1 + \Delta^2)^2$ that accounts for the presence of dilatational motion, and the crystal mode mass M_ν^Q. All of these parameters, except the liquid density, must be determined experimentally.

CHAPTER III

EXPERIMENTAL EQUIPMENT AND PROCEDURE

The series of crystals were rectangular quartz bars four times greater in length than width, with the thickness adjusted for the desired resonant frequency. Suitable electronic equipment was built to drive the unplated crystals and record the decaying mechanical vibrations. Figure 1 is a picture of the apparatus, and a block diagram of the electronic system is given in Figure 2. The equipment consists of three main parts.

3.1 Experimental Equipment

3.1.1 Pulse Forming Network. A pulse forming network was built to give pulses of variable length and separation. The network interrupts the continuous oscillator signal with the aid of a relay, and provides 20 milliseconds of pulse with an interruption of 100 milliseconds, which is long enough to record the complete waveform on a storage oscilloscope. The generator is connected parallel to the crystal at all times. The signal voltage applied to the crystal is 60 dB above its closed gate level.

The network consists of three IC chips and a Babcock relay. A closed loop CD 4001 AE multivibrator and its external circuit controls the repetition time and provides a 5-volt square wave triggering source for the 9601 monostable vibrator, whose external circuit controls the pulse width and drives the relay. A peripheral driver is inserted to increase the current to the relay. A five pf capacitor is inserted

Figure 1. Pictorial of the equipment.

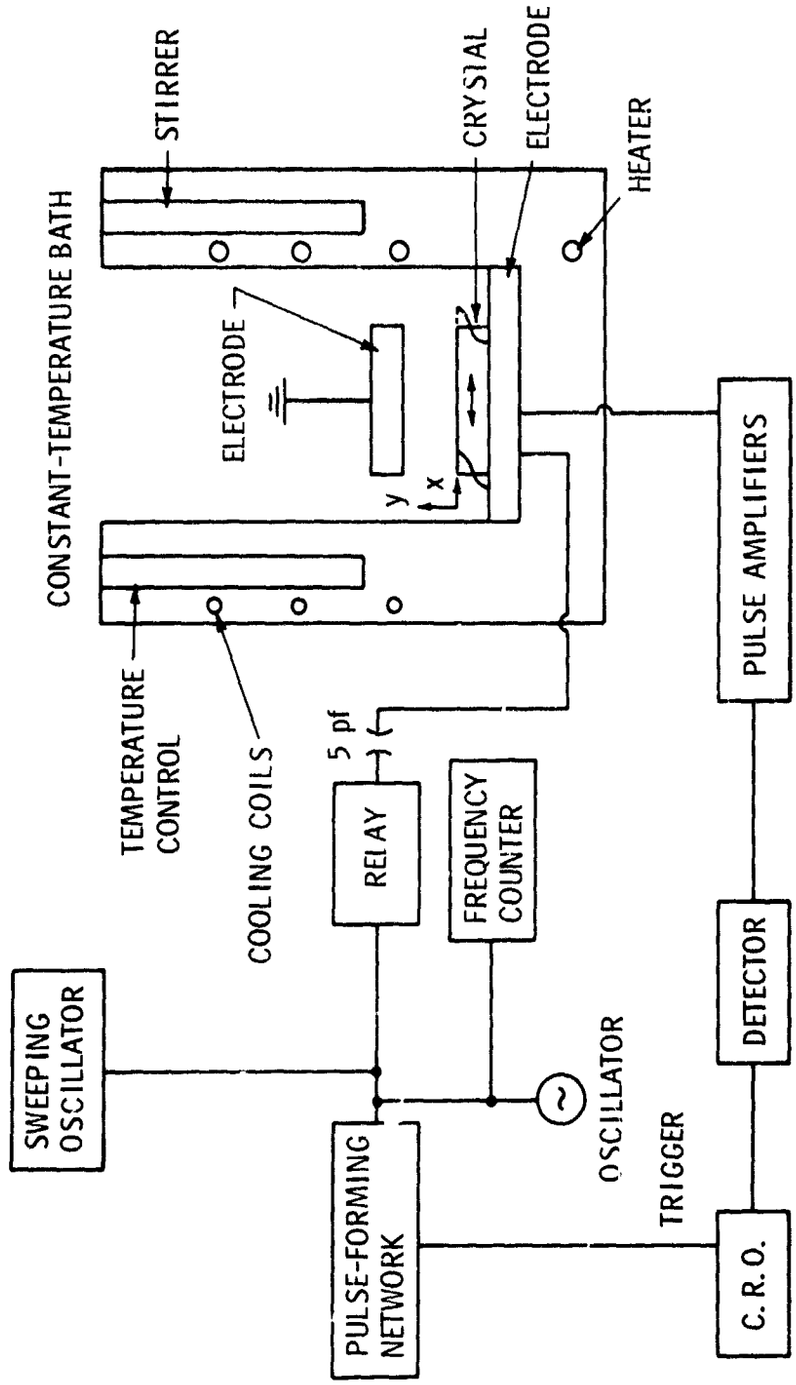

Figure 2. Block diagram of the electronic apparatus.

between the relay and the crystal to reduce decoupling the crystal whenever power is absorbed by the electrical equipment.

3.1.2 Temperature Bath. A twelve-gallon pyrex glass container with suitable heaters, stirrers, a thermocouple gauge, and cooling coils was built to control the temperature of the Ostwald-Fenske viscometers whenever measurements at larger liquid volumes were needed. The central portion of the bath was vacuum sealed and the essential parts of the shear viscometer were inserted and used to determine the correction factor (see Section 4.1.3). Measurements were also made of the effect of the unavoidable presence of adsorbed water on the crystal surface. The loss factor readings proved to be repeatable in both air and vacuum. Therefore, the shear viscometer was removed from the bath and placed on a separate stand to allow easier accessibility during measurement.

3.1.3 Pulse Amplifiers. A tuned pulse amplifier was built as an amplitude limiter to prevent the 2-volt driving pulse from saturating the 20 mv crystal output, since the same arrangement is used for driving and receiving. Figure 3 shows the circuit of the amplifier. Two silicon diodes in the input stage prevent the incident pulse from blanking out the amplifier. The 2N2222 transistors provide a gain of 680 over the frequency range from 200 to 620 kHz. Thereafter, the gain drops at a rate of 12 dB per octave largely due to the integrated circuits in the pulse forming network limiting the amplifier to frequencies below 2.0 MHz. The amplifiers amplitude response was determined by plotting $\frac{A_n}{A_n + 1}$ in dB versus time, where A_n is the decay amplitude n milliseconds after the start of the decay. The straight line response was indicative of a linear amplitude response

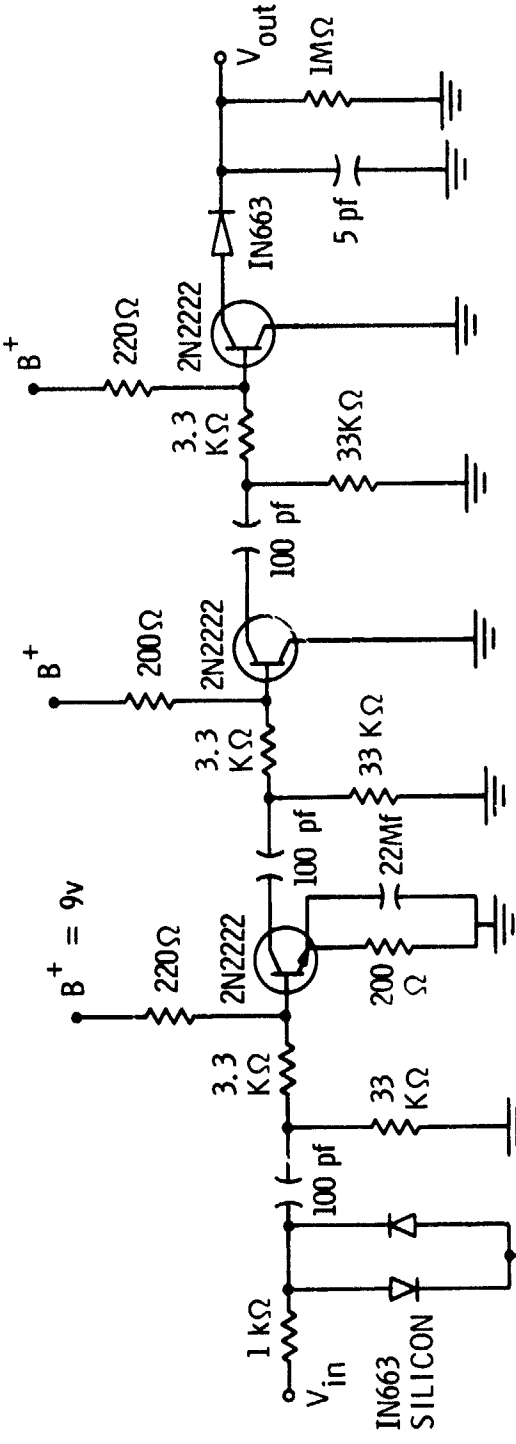

Figure 3. Electronic arrangement for the A.C. coupled pulse amplifier and detector.

over a wide range of amplitudes. In addition, the decay time of the amplifier was less than 1/10 of the normally measured decay times.

A demodulating detector forms the last stage of the amplifier. The low impedance of the detector to high frequencies permits the low frequency envelope to be displayed on the oscilloscope screen. The time constant of the detector was chosen so that the low frequency envelope coincided with the output of the last transistor stage.

A differential pulse amplifier was built and used to extend the measurement frequency to 10 MHz. The silicon diodes again serve as amplitude limiters to prevent overloading due to the driving pulse. The μA733 operational amplifiers give a fixed gain of 800 for the two stage amplifier. Figure 4 shows the circuit.

3.2 Experimental Procedure

3.2.1 Procedure During Measurement. Crystal specimens were made by Valpey Fisher Company to specifications required in this study (see Appendix B). The crystal was prepared for measurement by three repeated washings with ethyl alcohol and acetone. This procedure insured that the surface was free of any contamination that could prevent the crystal from being in good contact with the liquid. The crystals were excited while resting on a bottom base electrode, with the top electrode-crystal separation approximately 5.0 mm. A drop of liquid was then placed on the surface with a hypodermic syringe, and the decay time recorded. Since the decay was exponential, the amplitudes could be compared from the slope at any two points. The difference between this time constant (t_e) and the time constant when

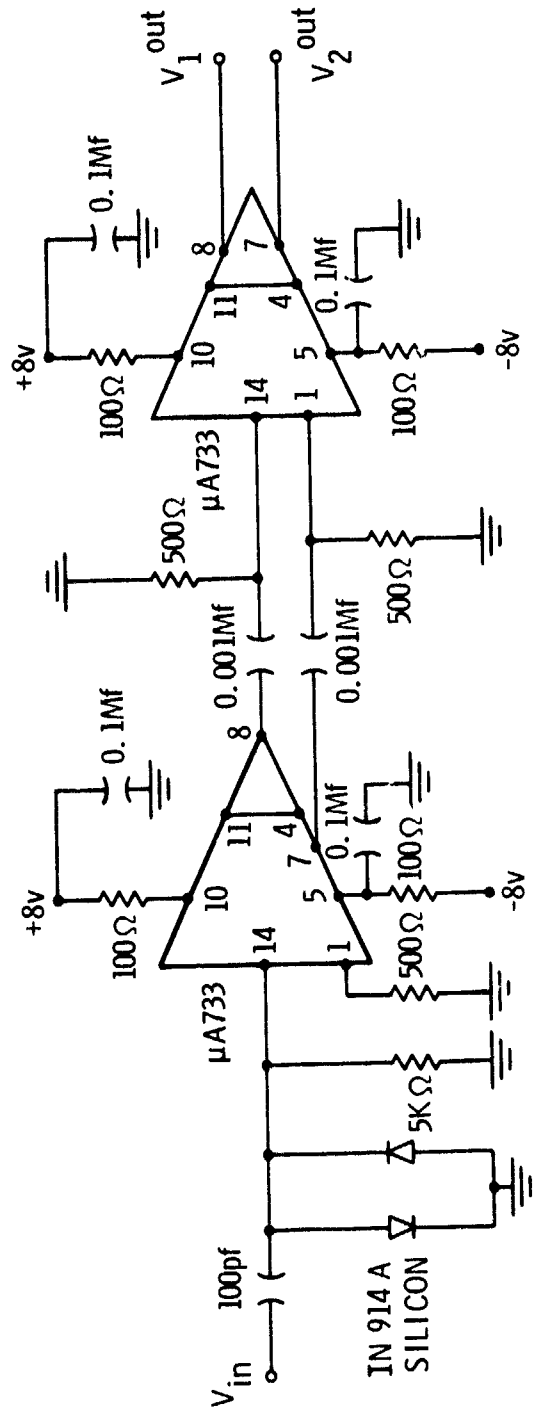

Figure 4. Electronic arrangement for the high frequency differential pulse amplifier.

the crystal is driven in air (t_e^0) is a measure of the effect of the liquid viscosity and yields a change of loss factor $\Delta\eta = \frac{2}{\omega\Delta t_e}$.

The crystal was earlier placed into a vacuum vessel to eliminate sound radiation and the relative energy of the dilatational component of vibration determined. The resonant frequency ω was measured with a GR 1163-A coherent decade frequency synthesizer to an accuracy of 1/10 Hz. The liquid surface contact area σ_L was measured with a microscope with an accuracy of 0.01 cm^2. The crystal mode mass was the final value needed in Equation (2.27), and was determined (see Section 4.1.5) to be $\frac{1}{2\sqrt{2}}$ times the crystal mass M^Q.

As an example of a particular measurement, the decay time in air was measured as (58 ± 1.0) ms at 502 kHz, giving a loss factor of $(1.09 \pm 0.02) \times 10^{-5}$. Placing S-20 oil, of contact area 0.155 cm^2, on the crystal surface, decreases the decay time to (22 ± 1.0) ms and increases the loss factor to $(2.87 \pm 0.14) \times 10^{-5}$. The effect of the oil increased the loss factor by $\Delta\eta = (1.78 \pm 0.12) \times 10^{-5}$. For 502 kHz, the static mass of 4.35 gms gave a mode mass of 1.53 gms. The correction factor, from Table II, was 1.63. Thus, the viscosity of the oil droplet was (39.4 ± 5.4) cp. The uncertainty of the viscometer was 14% in this particular measurement. In most cases, the accuracies were better.

3.2.2 Procedure for Red Blood Cell Deformability Studies. Bovine blood was used as the source of red blood cells in this study. The blood was collected immediately after the aorta was cut, and one part

of anti-clotting solution consisting of 13.4 gms of sodium oxalate in 1.0 liter of water was added to nine parts of whole blood. The whole blood was then centrifuged at 4000 rpm for 15 minutes so that the heavier red cells could be separated from the lighter plasma with a thin layer of white blood cells remaining in between. Both the plasma and leukocyte layer were syphoned off and discarded while the red cells were placed in an equal volume of saline solution and washed twice. The washed red cells were then combined with a normal saline suspension, and the hematocrit adjusted for desired cell volume. This was especially important since the absorption of shear waves can be attributed to proteins in the red cells and hemoglobin is the most abundant protein in blood (10).

Chemicals were used to change the deformability of the erythrocytes. Sodium Oleate changed the rheological properties of the erythrocytes through changes in cell shape, resulting in changes in the surface area to volume ratio. Acetaldehyde is known to increase the tension of the outer membrane of a red cell with a consequent reduction in surface area. The preparation procedure was as follows: 1) Two grams of sodium oleate were added to 100 milliliters of a normal saline solution, and 5 ml of this solution was added to 500 ml of red cells resuspended in saline. 2) Ten milliliters of acetaldehyde were added to 324 ml of normal saline. This solution was then added to 666 ml of similarly packed red blood cells to make one liter of 1% acetaldehyde suspension.

Due to the great effect of hemolysis on deformability, a time limit of 8 hours was established, during which all measurements were performed

The frequency behavior of droplets of blood containing these resuspended cells was measured with the shear viscometer by measuring the decay time. The results were compared to available Brookfield data (11) at the physiologically low shear rates from 0.15 to 73 1/sec.

CHAPTER IV

EXPERIMENTAL RESULTS

4.1 Basic Research

4.1.1 Frequency Response and Quality Factor of the Crystals. The frequency spectrum was examined for crystals vibrating in air at their resonant mode, with a typical result given in Figure 5 for 283 kHz. The figure shows a clear, single response of the amplitude and its accompanying sidebands. Spurious modes are absent within 40 Hz on either side of the fundamental. This is a critical result, since adjacent modes have their own velocity distribution and dilatational components. The troublesome neighboring modes have been eliminated by proper dimensioning, as discussed in Appendix B.

The figure also shows the response of the crystal with a drop of NBS oil S-20 (static viscosity, 38.7 cp) on its surface. The oil decreases the resonant frequency by 10 Hz and suppresses the sidebands completely.

To insure that contributions of modes whose frequency is different from the driving force may be neglected, a crystal vibrating in air should have a large quality factor of resonance Q. The quality factor of the crystals was plotted from 0.1 to 0.5 MHz at their fundamental frequencies and from 0.6 to 1.0 MHz at an odd harmonic of the fundamental frequency. A typical result was 10^4 at 0.5 MHz.

4.1.2 Support of the Crystal. Suitable crystal supports were needed to insure unrestrained vibrations of all shear modes and prevent the generation of a secondary frequency spectrum. An unstable crystal

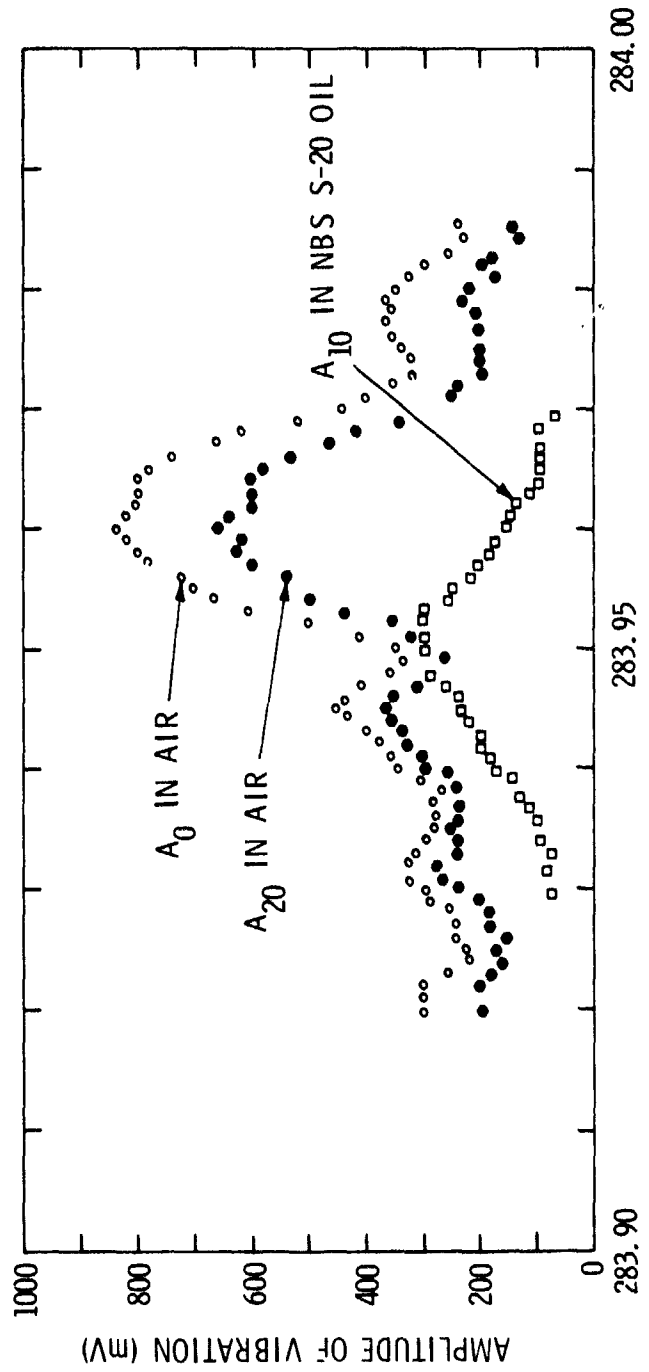

Figure 5. Amplitude zero and twenty seconds after start of decay in air, a 1 ten seconds after start of the decay in S-20 oil.

mounting system could also cause a lack of reproducibility during measurement. The quality of a certain suspension can be ascertained from a plot of the amplitude of vibration A_0^2 for various relative changes of the frequency $\Delta\omega/\omega$. The results for razor blades, phonograph needles, and a plane metal base are shown in Figure 6. The figure shows that the best support arrangement is to simply rest the crystal on the brass base with the crystal essentially suspended by an elastic air cushion. Furthermore, the microscopic air layer eliminated sound radiation from the bottom crystal surface.

4.1.3 Effect of the Electrodes on the Vibration of the Crystal. The lower electrode is formed by the metal base of the crystal holder. The upper electrode is electrically separated from the bottom base by four insulated support rods and can be adjusted vertically by a micrometer screw accurate to .01 mm. The air gap between the crystal working surface and the top electrode acts as a low loss, rigidly reflecting wave guide.

Standing waves can be expected to influence the quartz vibration by introducing interferences that depend on the distance of separation Figure 7 is a plot of the quality factor versus electrode separation, from 0.25 to 30 mm, for three different loading conditions, vacuum, air and water droplets. The maxima in this figure are caused by interferences from standing waves. The difference in the value of Q when the crystal was very close (0.25 mm, so that sound radiation was eliminated) to a position very far away (i.e., 30 mm) is a rough indication of the amount of sound radiated.

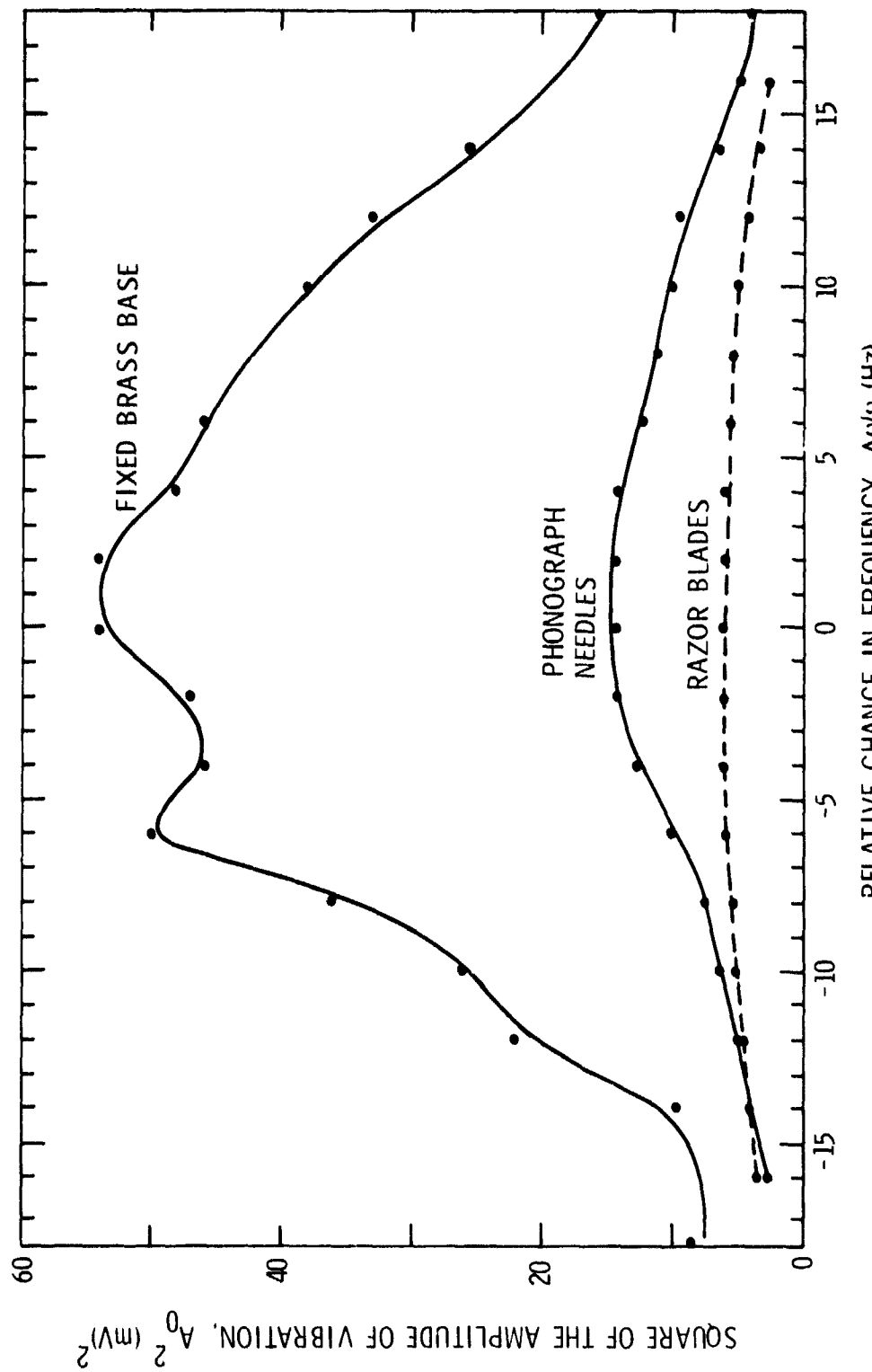

Figure 6. Resonance curves of a vibrating quartz crystal for the following supports: 1) fixed brass base, 2) phonograph needles, 3) razor blades.

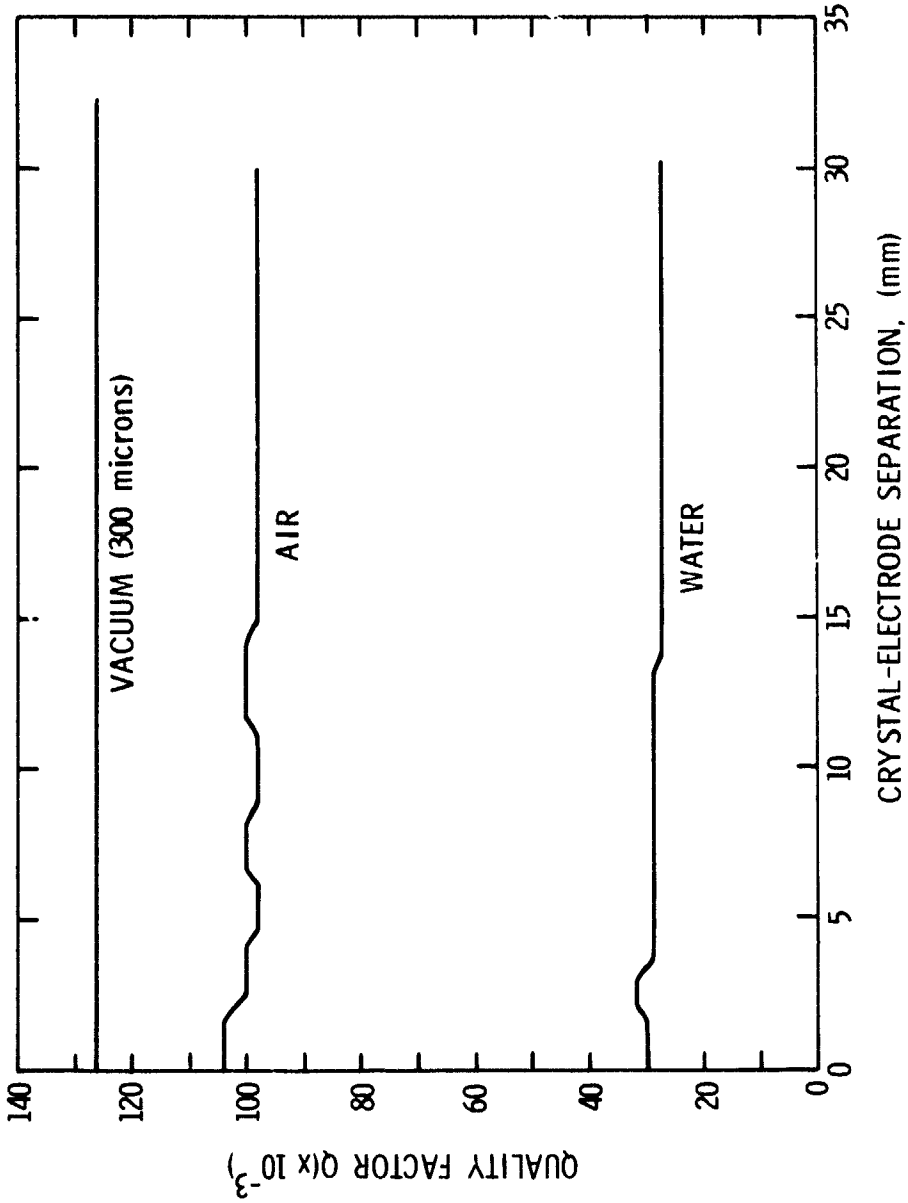

Figure 7. Quality factor versus distance of separation between top electrode and crystal surface at 503 kHz for vacuum, air, and water loading.

A more accurate measurement can be obtained by examining the change in the quality factor in air and under 300 microns of vacuum when the top electrode is very far away (e.g., 30 mm). The correction factors in Equation (2.27) would thus be determined for all crystals. Table II shows that the results for 0.5 MHz was $\Delta = 0.33$ and $(1 + \Delta^2)^2 = 1.23$. Crystals numbered 2 and 4 were rejected because the dilatational component relative to shear was too great.

4.1.4 Effect of Pulse Duration and Temperature. The influence of the relay on the decay measurements was considered. At the moment the power is switched off, the relay could be at a point of maximum velocity or maximum amplitude, or somewhere in between. The amplitude decay $Ae^{-\delta t}$ may therefore depend on the phase of the relay.

The switching on and off also generates undesired transients To see whether they have any effect on the decay amplitude, the pulse duration was varied. Figure 8 illustrates the decay curves for different pulse duration irrespective of the phase at the moment the power is switched off. The linear response of the amplitude indicates that transients and phase of power switch off do not influence the results.

The influence of increasing the temperature on the viscosity measurements was examined by varying the time of measurement. Figure 9 shows the results for drops of water at 0 5 MHz The decrease in viscosity at 200 and 500 seconds after the drops have been placed on the crystal surface is due to the increased temperature resulting from the large number of pulses striking the crystal Both drops approach a thin film geometry because of evaporation as seen from the maxima in

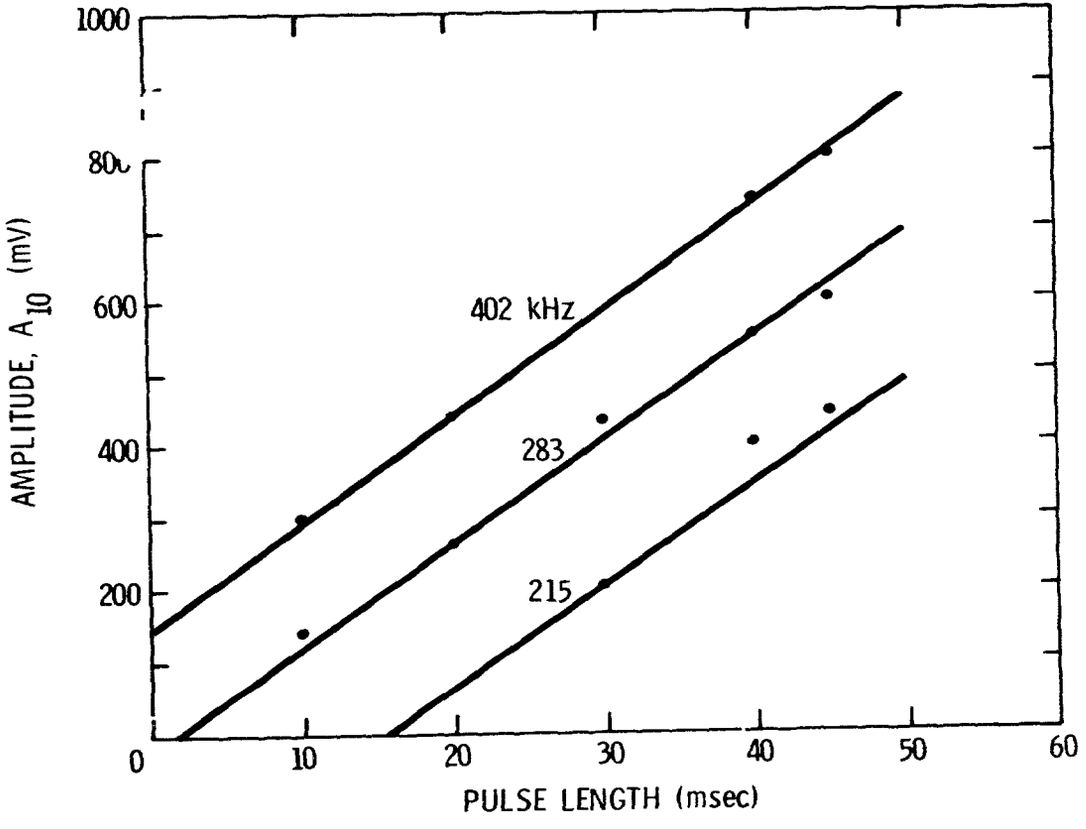

Figure 8. Amplitude ten seconds after the start of decay versus pulse length for three frequencies.

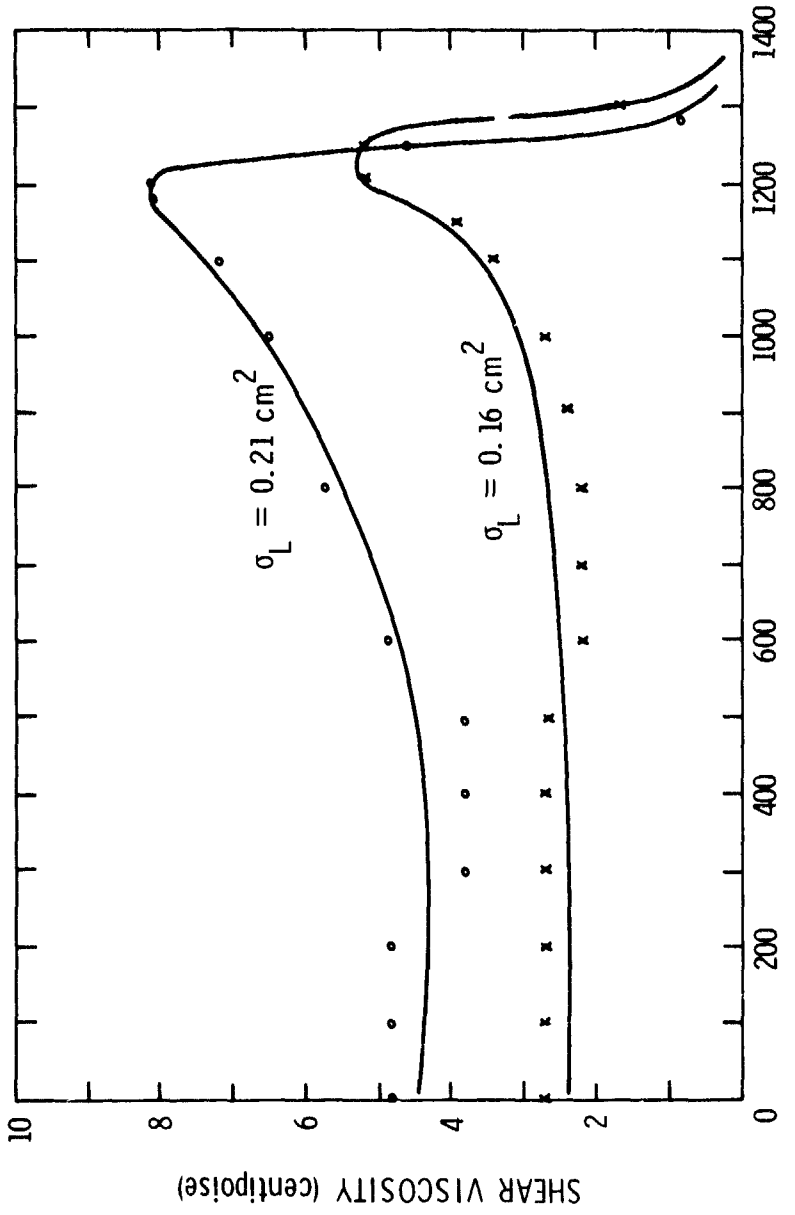

Figure 9. Shear viscosity of water versus time (or thickness) for two liquid contact areas at 503 kHz.

Table II. Ratio of dilatational component to shear component, and correction factor $(1 + \Delta^2)^2$ versus frequency.

Crystal #	Frequency (kHz)	$\Delta = \frac{V_{dil}}{V_{sh}}$	$(1 + \Delta^2)^2$
1	235	0.52	1.63
2	282	1.25	6.65
3	283	0.57	1.74
4	296	1.44	9.47
5	402	0.33	1.23
6	503	0.32	1.23
1	602	0.55	1.69
1	704	0.51	1.57
1	997	0.32	1.21

the viscosity curves. Care was taken to finish all measurements within 200 seconds.

4.1.5 Effect of Velocity Distribution Over the Crystal Surface

It is a very difficult task to determine the transverse velocity of small crystal bars, since the displacement amplitude is of the order of 24 Å/1 volt at 500 kHz. There is also no reason to believe that the crystal vibrates with a uniform velocity. Previous authors (12) have treated the crystal velocity distribution as a one-dimensional problem, with the displacement varying harmonically along the y axis, $\xi = \xi_0 \sin(ky-\omega t)$, giving an effective crystal mass of $M_v = \frac{1}{2} M^Q$. The particular transverse velocity distribution also determines the loss factor for the liquid through its dependence on the inverse square of the liquid surface velocity amplitude.

Probably the most accurate method of determining the mode mass is to place small drops at various positions on the quartz surface and determine the local velocity from the resulting decay time. A position of larger shear motion is indicated by a short decay time, and a minimum of motion is detected by a longer decay time. The loaded crystal would have a diminished amplitude, yet retain the displacement pattern of a free surface.

This has been done for glycerol drops and the results are represented in Figure 10. For a vibrating quartz bar the velocity is a maximum at the center and decreases towards the boundaries of the plate. This means that some parts of the plate surface take no part in the motion and the average velocity must be determined from the square root of the local viscosity. The one-dimensional mode mass is therefore closer to $\frac{1}{2\sqrt{2}} M^Q$ than $\frac{1}{2} M^Q$. Similar distributions were measured for all four crystals.

The variation of velocity with width was determined by mapping the two-dimensional surface of the crystal. A sharply pointed cone was held fixed while the lower crystal support was driven in the horizontal plane by two clock motors through a suitable gear arrangement. The cone functioned as the top electrode as well as a probe, simultaneously applying piezoelectric excitations locally. The crystal surface was mapped by synchronizing the signal of the stationary upper electrode with an oscilloscope sweep and the decay amplitude measured as a function of position on the two-dimensional surface. The central region was again a maximum of shear motion, with a drop off near the outer width boundaries influenced by the decreasing number of flux lines

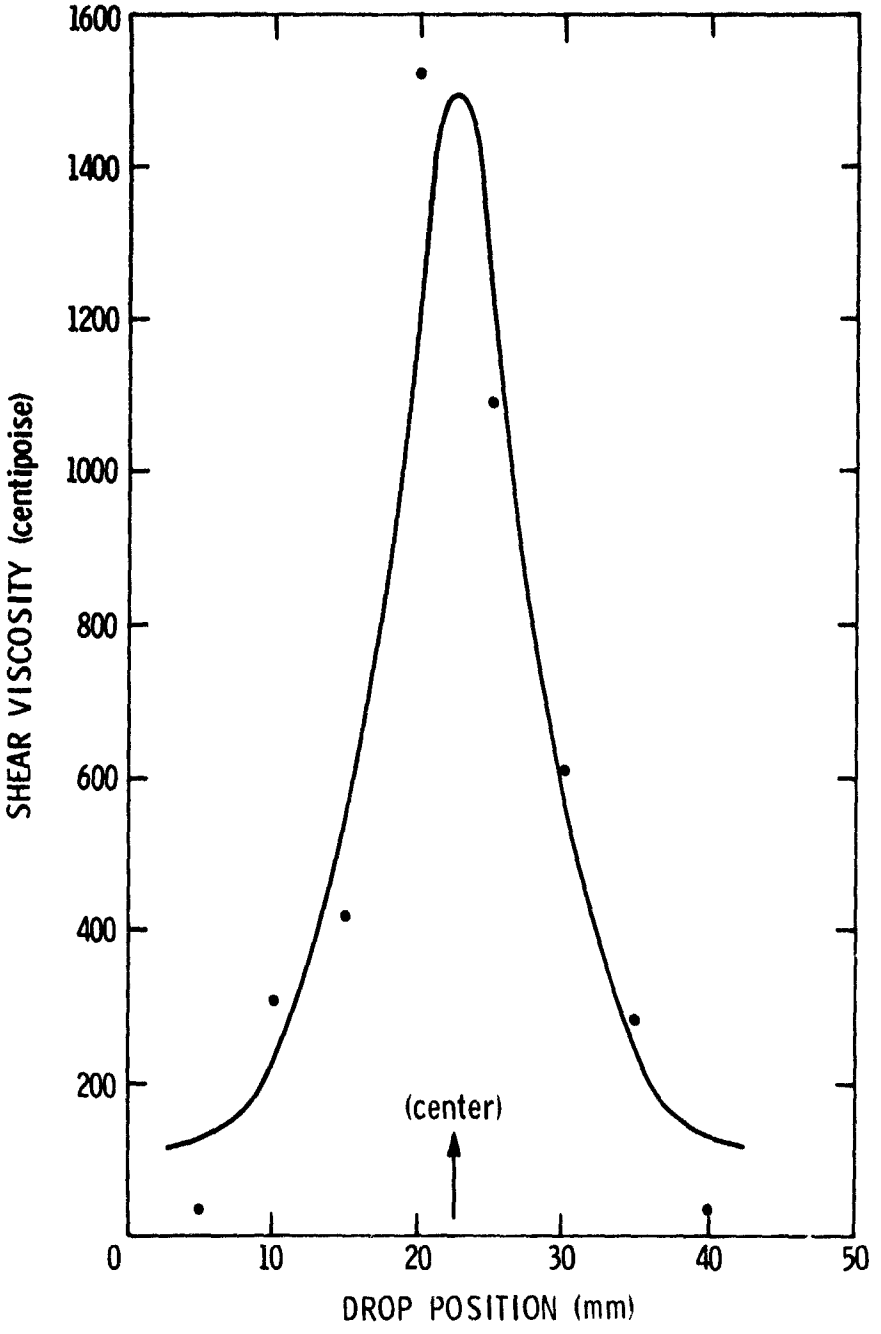

Figure 10. Shear viscosity of glycerol drops at different positions on the crystal surface, at 283 kHz.

reaching the crystal surface. The results show that the vibrational velocity does not vary much with the width since the width was so relatively small compared to the length. Extensive measurements by Sykes on Y-cut quartz plates have shown that the velocity distribution is practically independent of the width (13).

4.1.6 Effect of Contact Area of the Liquid. Previous authors (14) have found that energy losses in liquids were significantly influenced by the liquid contact area σ_L. In this study, extensive measurements were made of viscosity as a function of liquid contact area, and a pattern began to emerge. Figures 11 to 14 show the results for drops of water. The peaks in the viscosity of water were due to compressional resonances that generate a relative motion parallel to the surface of the crystal, and result in additional shear losses. The peaks were therefore ignored, and the viscosity was determined from the minima of the curves after repeated measurements were made on each sample. The results for glycerin and urethane varnish are shown in Figures 15 and 16.

4.1.7 Effect of Surface Tension. It was possible to increase the volume of the liquid without changing the contact area by placing smaller drops on top of each other. In this manner, the radius of curvature and the effect of surface tension was increased. Also, the surface tension could be decreased by adding drops of detergent to 100 ml of water. No significant change of the viscosity could be observed, although the viscosity versus drop area data became scattered. It is possible that the method used to increase the volume (by placing drops on top of each other) was not sensitive enough to isolate surface

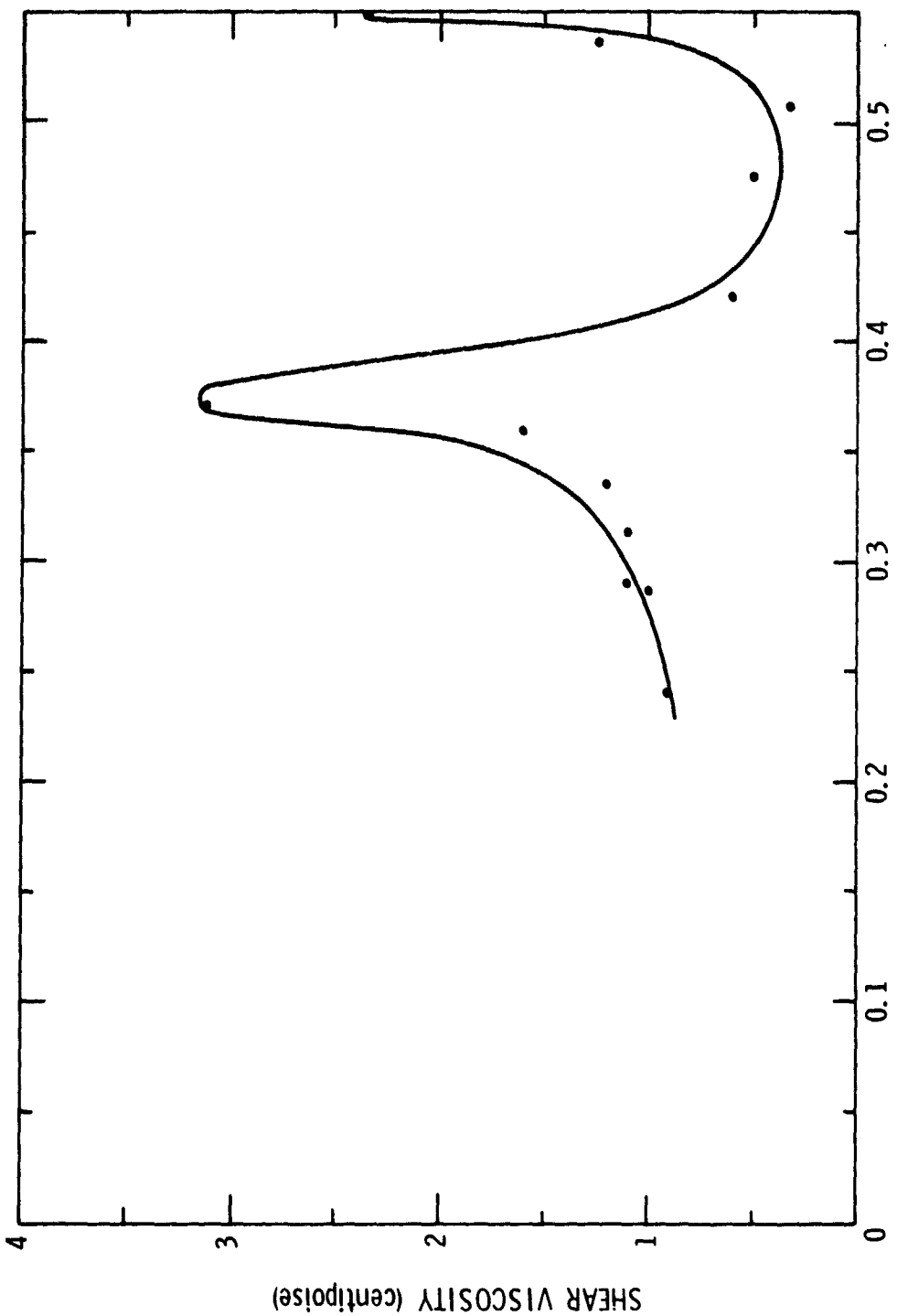

Figure 11. Shear viscosity of water versus surface contact area, at 235 kHz.

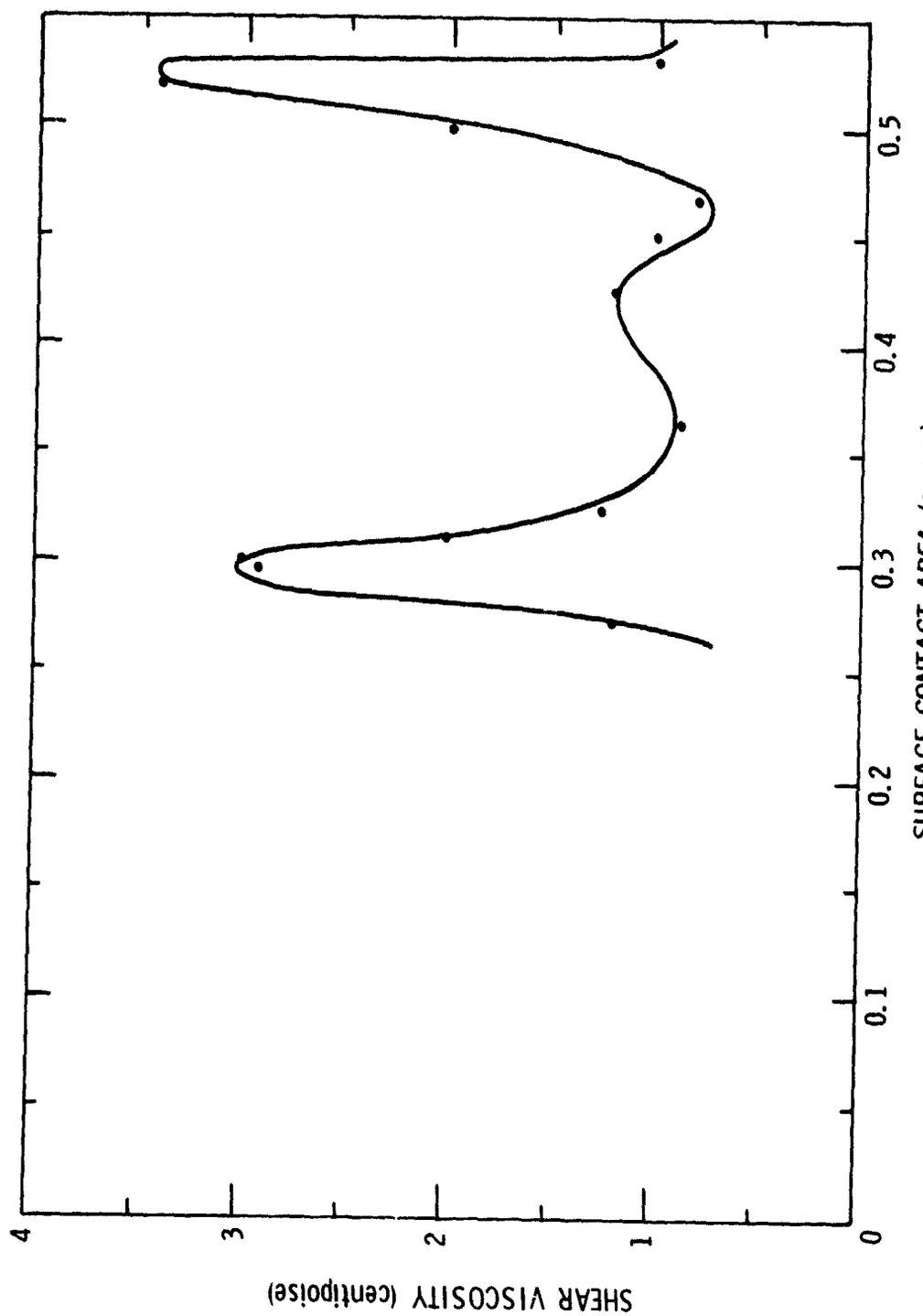

Figure 12. Shear viscosity of water versus surface contact area, at 283 kHz.

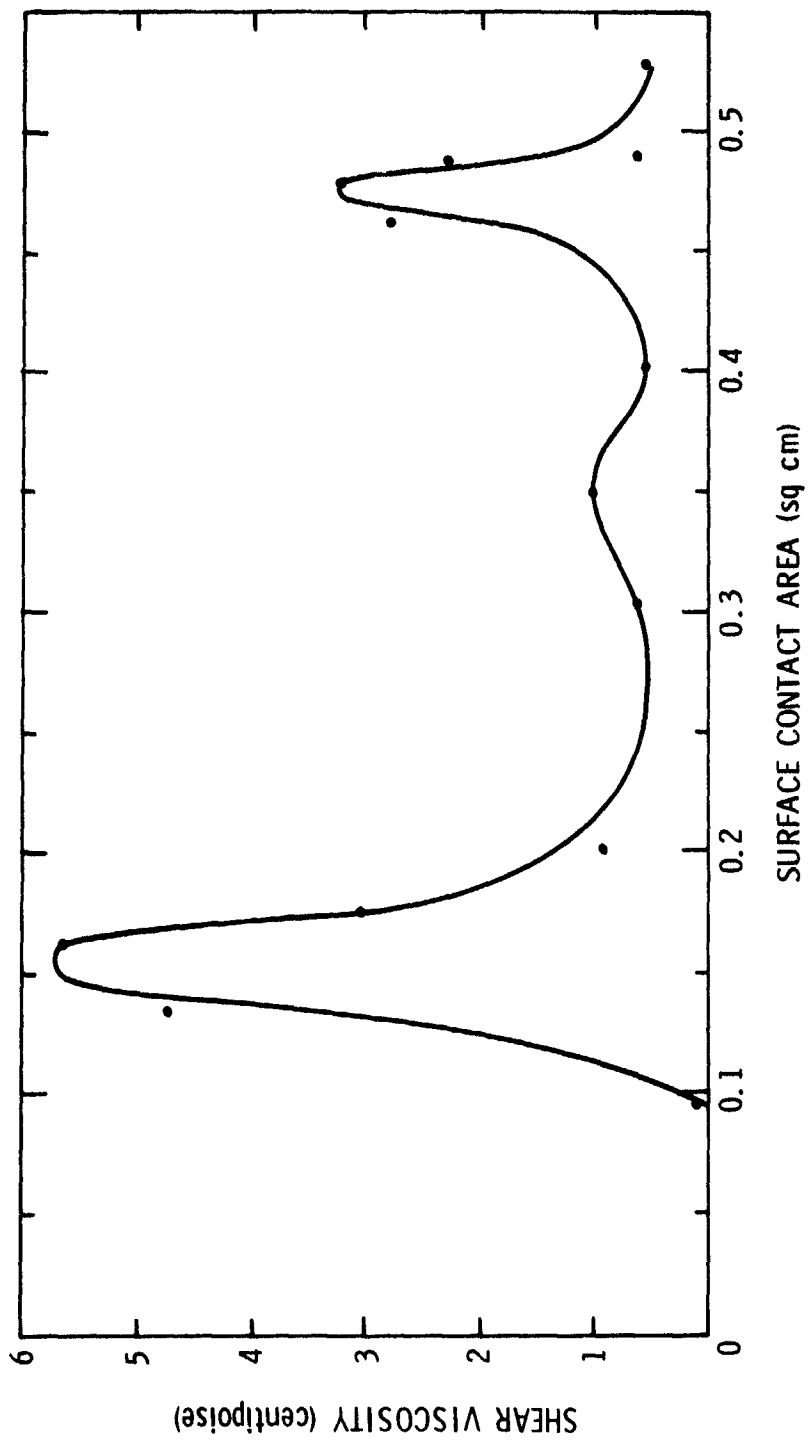

Figure 13. Shear viscosity of water versus surface contact area, at 402 kHz.

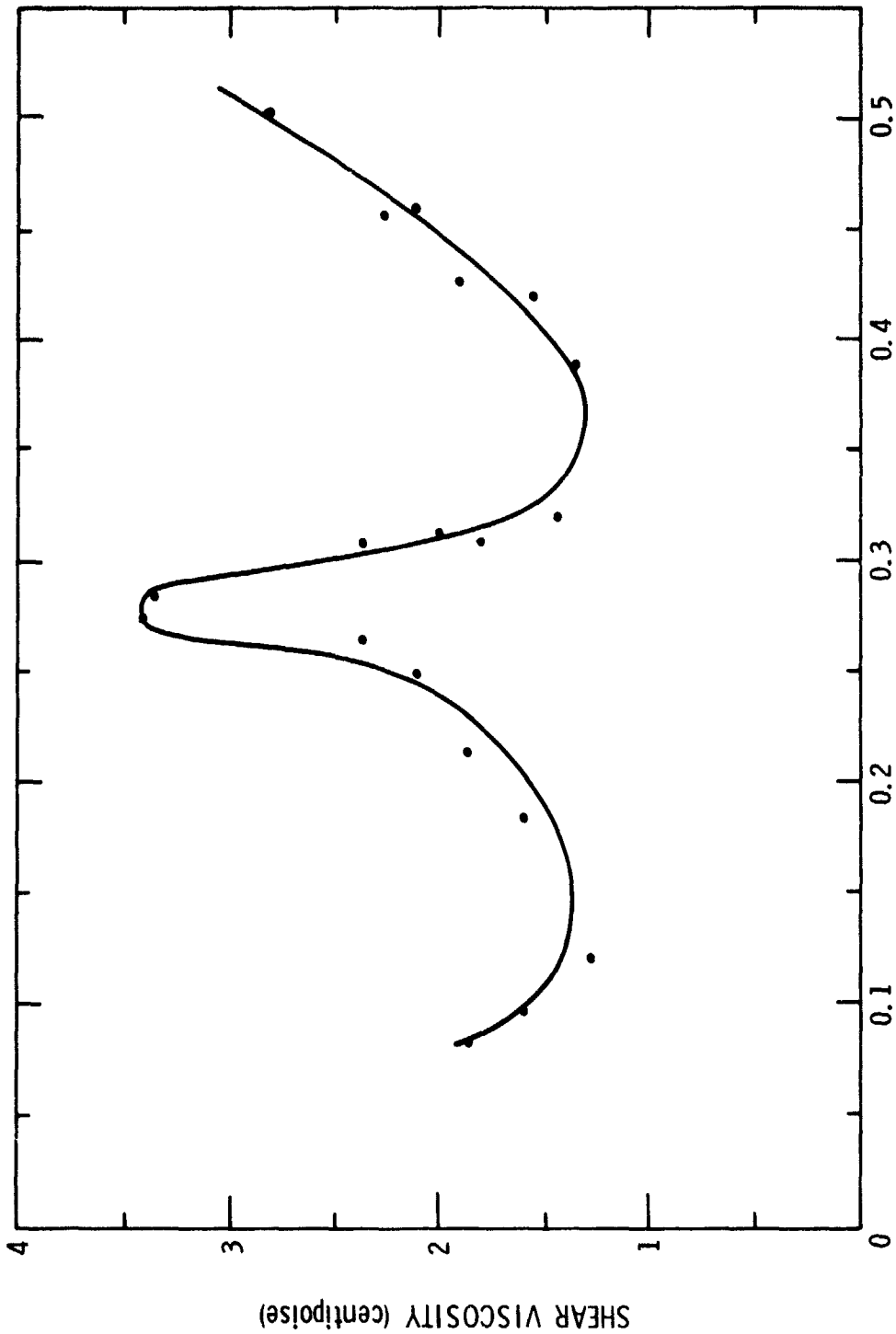

Figure 14. Shear viscosity of water versus surface contact area, at 503 kHz.

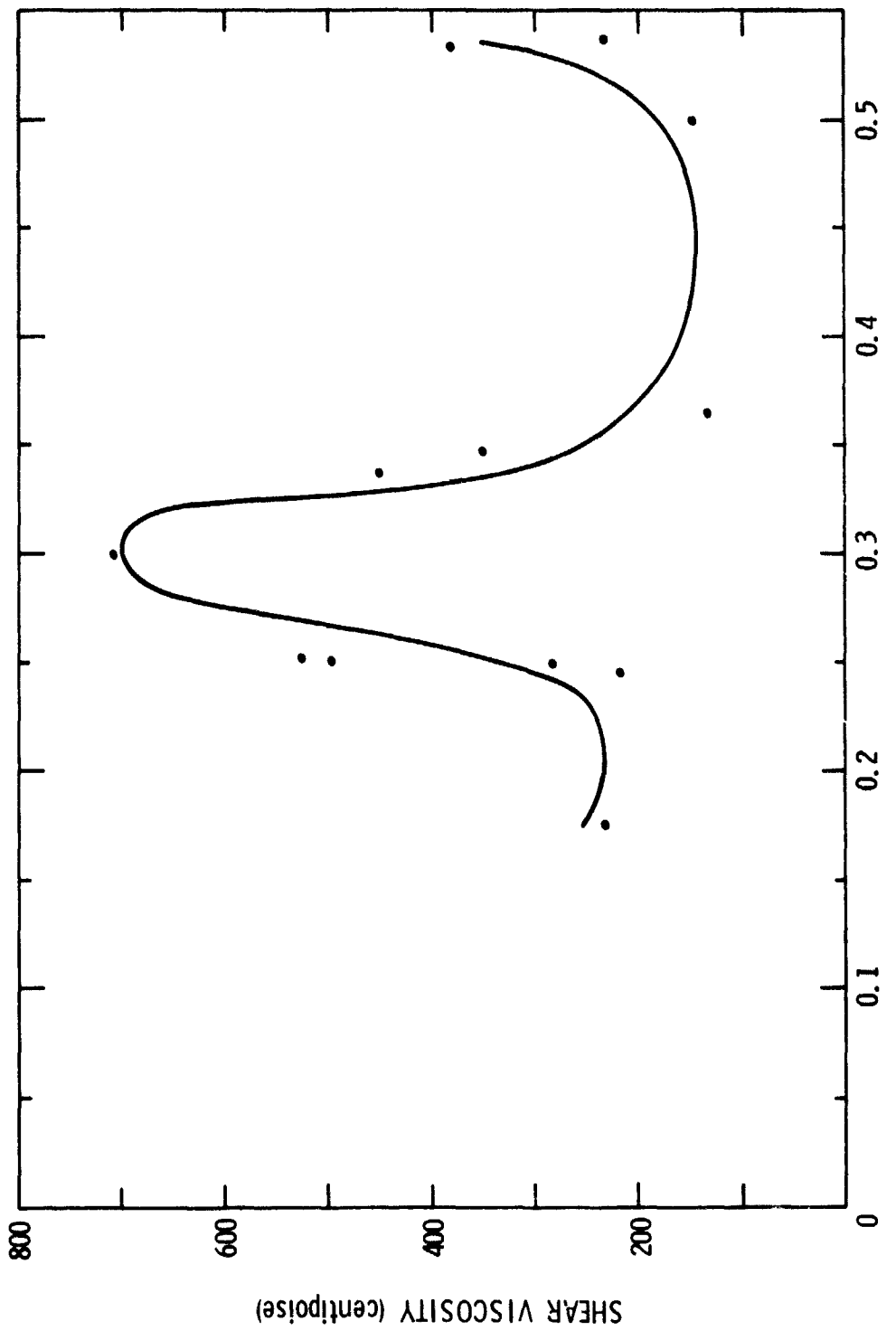

Figure 15. Shear viscosity of glycerin versus surface contact area, at 283 kHz.

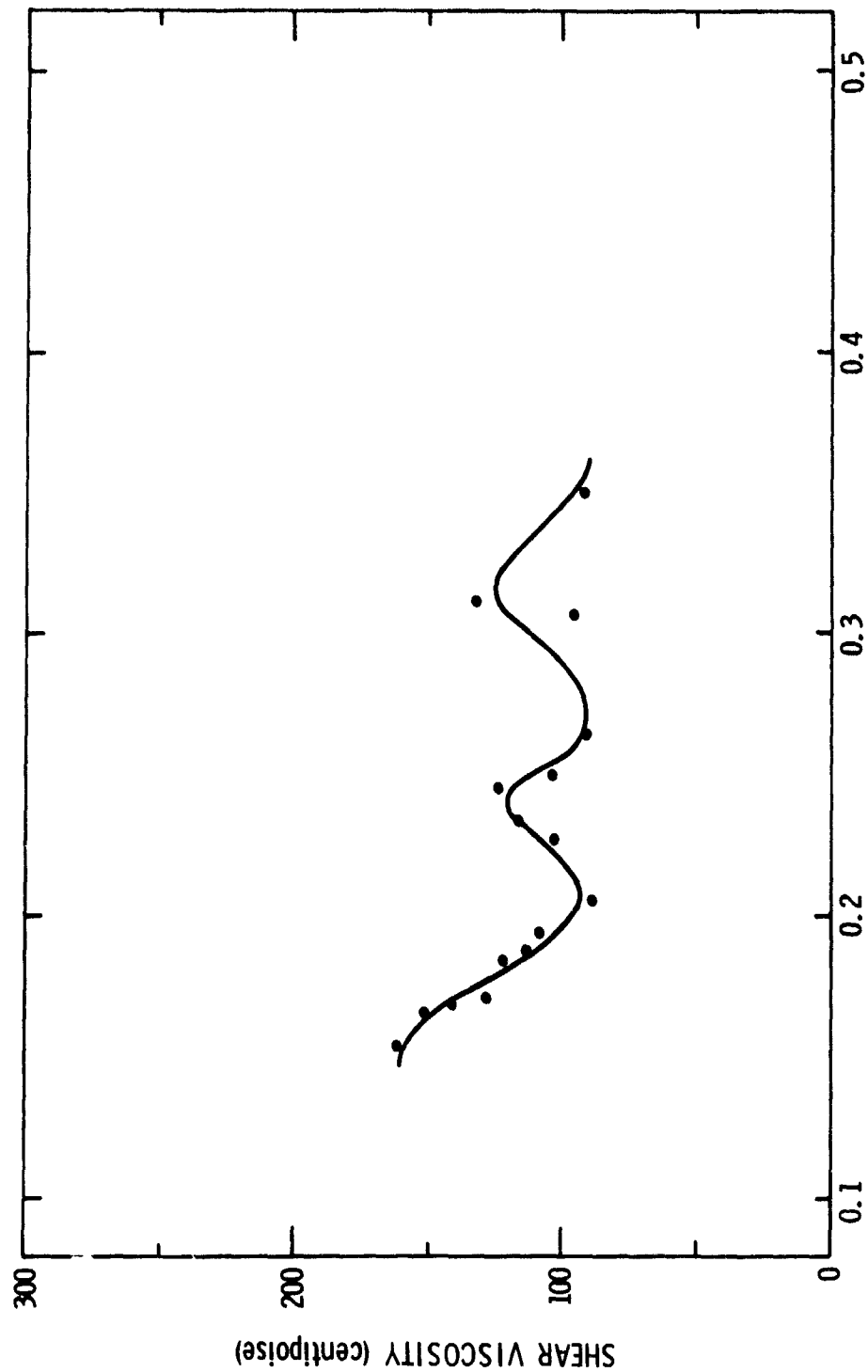

Figure 16. Shear viscosity of satin XL-8 urethane varnish versus surface area, at 402 kHz.

tension effects in the presence of compressional droplet resonances. In fact (see Section 4.2) when the viscosity was later measured at different frequencies, it seemed that the increase of droplet viscosity around 400 kHz was due to surface tension. This increase in the viscosity at higher frequencies was evident for all the liquids that were measured. Klemm (15) has shown that surface tension could increase the viscosity losses by a factor as great as 10,000. It would therefore not be surprising that a two-fold increase in the viscosity could occur and consequently superimpose a scattering on all the liquids measured. A greater clarification could only be brought about by building equipment specializing in surface tension effects.

4.2 Measurements of the Viscosity of Normal Fluids

4.2.1 Water. It seemed reasonable to believe that a calibration liquid was needed to determine the surface losses of each crystal, and then refer all other liquid results to this fluid. Work performed earlier with glycerin was rejected when the viscosity of glycerin was found to be strongly dependent on the water content and varied greatly over a relatively small temperature range. Water was finally chosen as the most suitable calibration fluid and the results from 0.235 to 1.0 MHz are are shown in Figure 17. The viscosity of droplets of water is close to the static value of 0.89 at 25°C for all values except in the range from 0.4 to 0.5 MHz. The increase in the droplet viscosity is greater than the uncertainty of the measurement and is not due to the molecular properties of water since any relaxation phenomenon should show a decrease with frequency. It is likely that the increase in droplet viscosity is due to surface tension. The surface tension

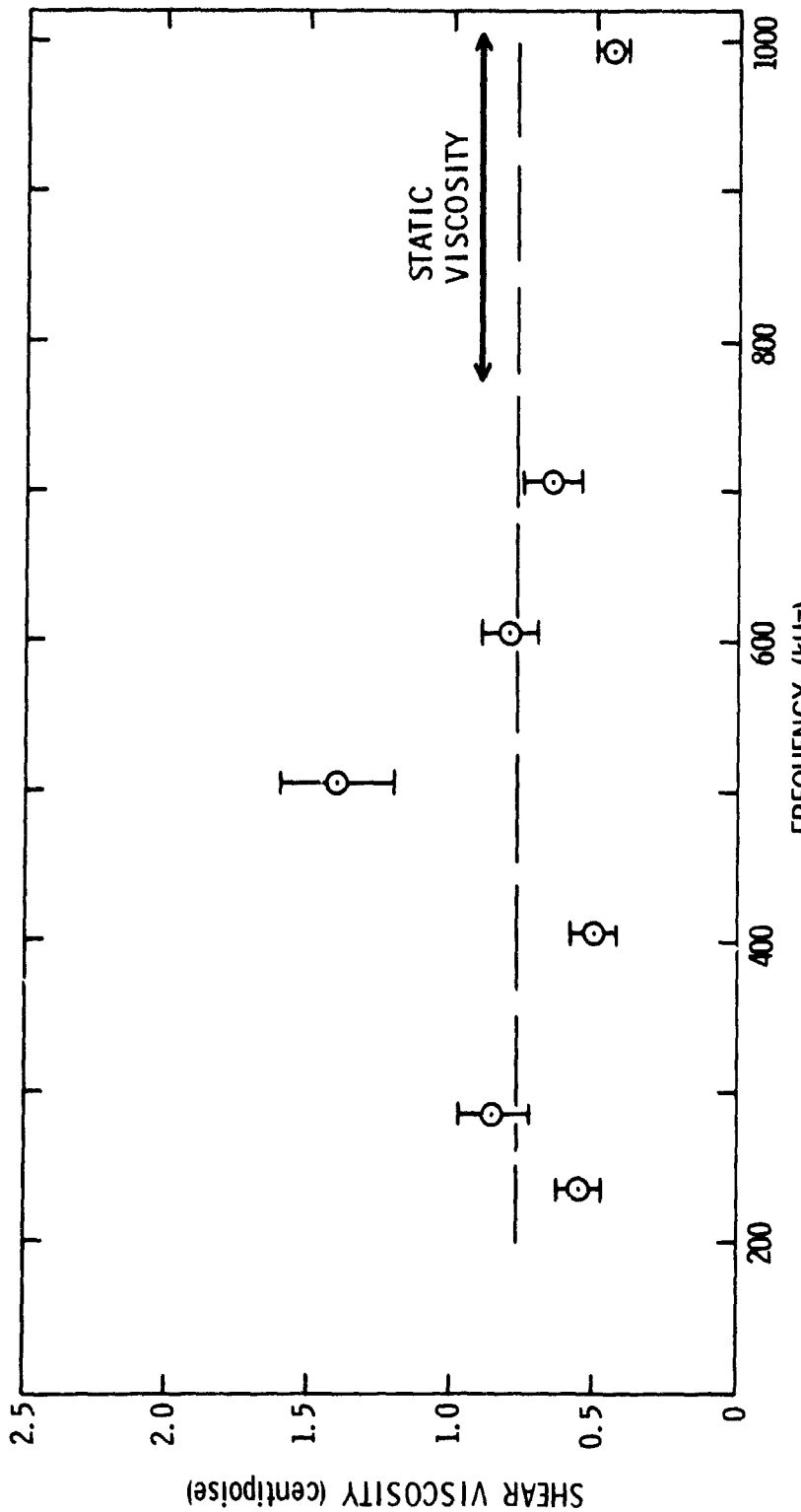

Figure 17. Shear viscosity of water from 0.235 to 1.0 MHz.

effect was evident in all liquid droplets that were studied, except possibly the bonding agents. It was therefore not possible to refer the experimental results to water and absolute measurements were preferred.

4.2.2 NBS Oils S-20 and S-600. The viscosity of NBS oil S-20 was measured over the frequency range from 0.283 to 1.0 MHz. The results in Figure 18 are scattered about the static viscosity of 38.7 centipoise presumably due to surface tension.

NBS oil S-600 was measured over the same frequency range, and the results are shown in Figure 19. For frequencies below 0.4 MHz, the results are near the static value of 1425 cp at 25°C. However, starting at 0.4 MHz, the viscosity decreases dramatically and scatters about the lower value of 400 cp. This decrease in viscosity may be due to molecular relaxation, which is possible for these high viscosities.

4.2.3 Varnish and Cedar Wood. The viscosity of Satin XL-8 urethane varnish was also measured over the frequency range from 0.235 to 1.0 MHz, and the results are shown in Figure 20 Below 0.6 MHz, the viscosity scattered about the constant value of 73 cp, slightly greater than the static value of 60 ± 5 cp. At 1.0 MHz, the viscosity was 19.5 cp. This large decrease in the viscosity may be due to absorption of energy in the long molecular chains of the polymer base of urethane varnish, and indicate the presence of relaxation phenomenon.

The results for cedar wood oil are given in Figure 21. The viscosity was greater than the static value by nearly 17 cp possibly due to surface tension. Table III lists the results for water, S-20, S-600, varnish and cedar wood oil

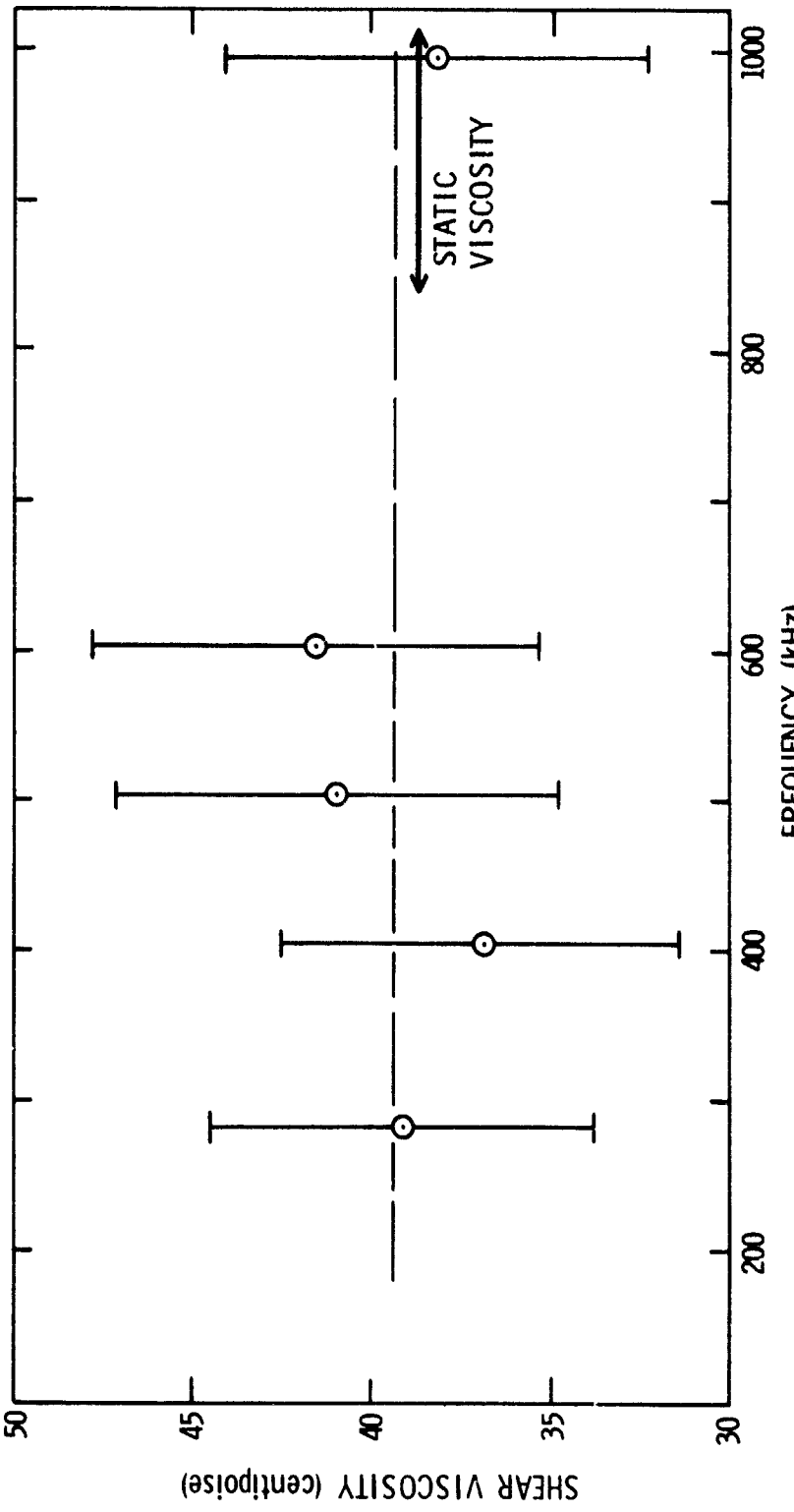

Figure 18. Shear viscosity of NBS oil S-20, from 0.283 to 1.0 MHz.

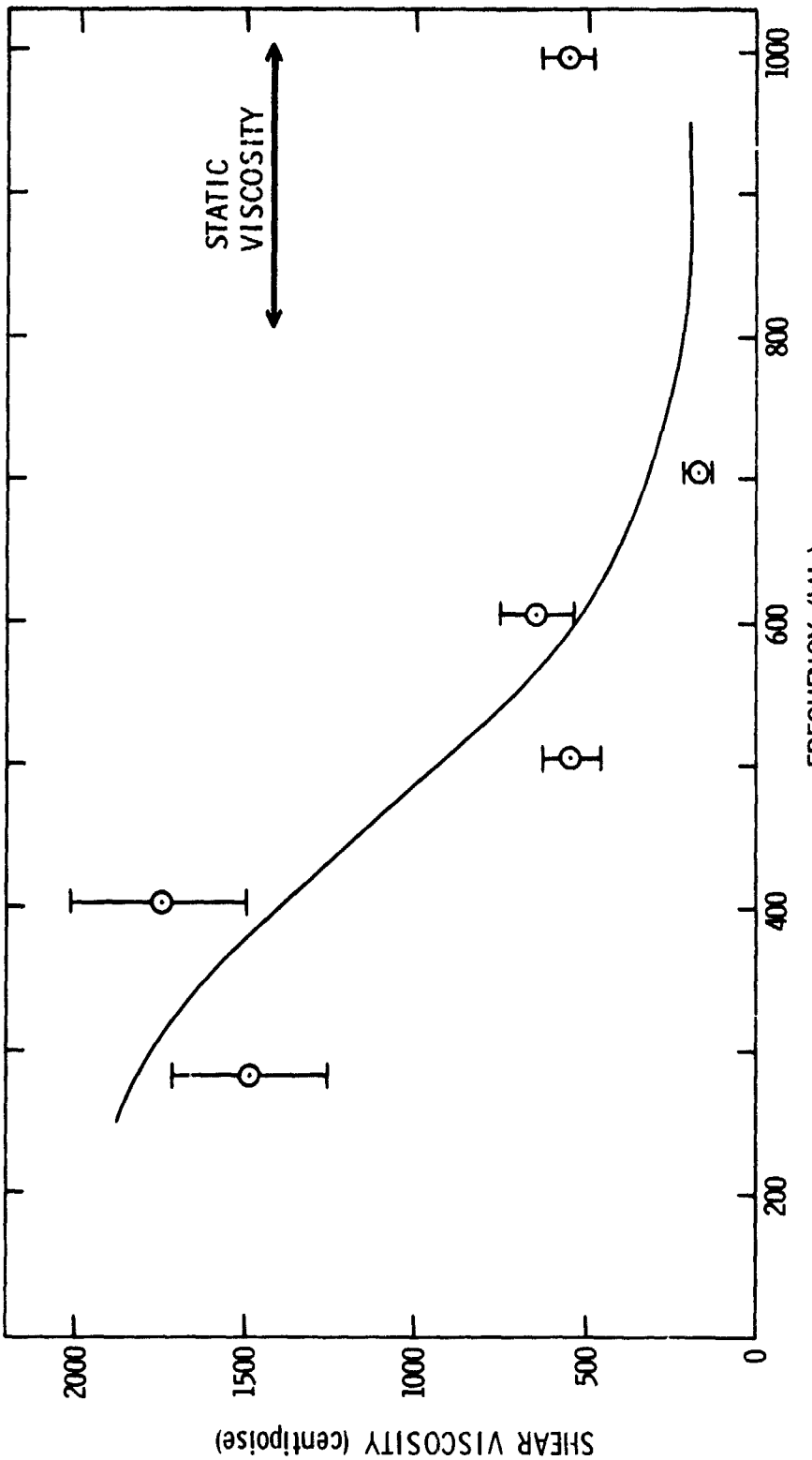

Figure 19. Shear viscosity of NBS oil S-600, from 0.283 to 1.0 MHz.

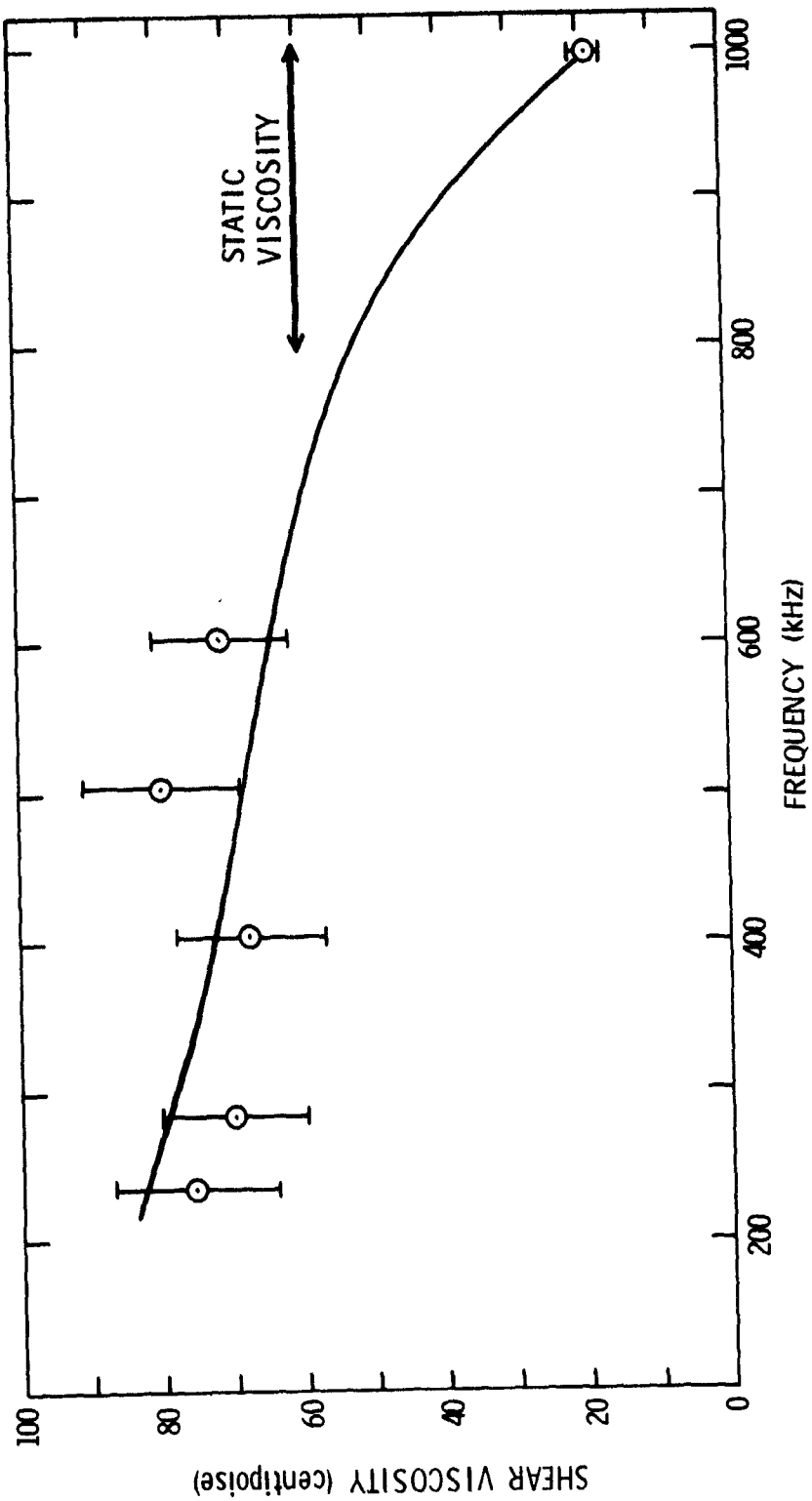

Figure 20. Shear viscosity of urethane varnish, from 0.235 to 1.0 MHz.

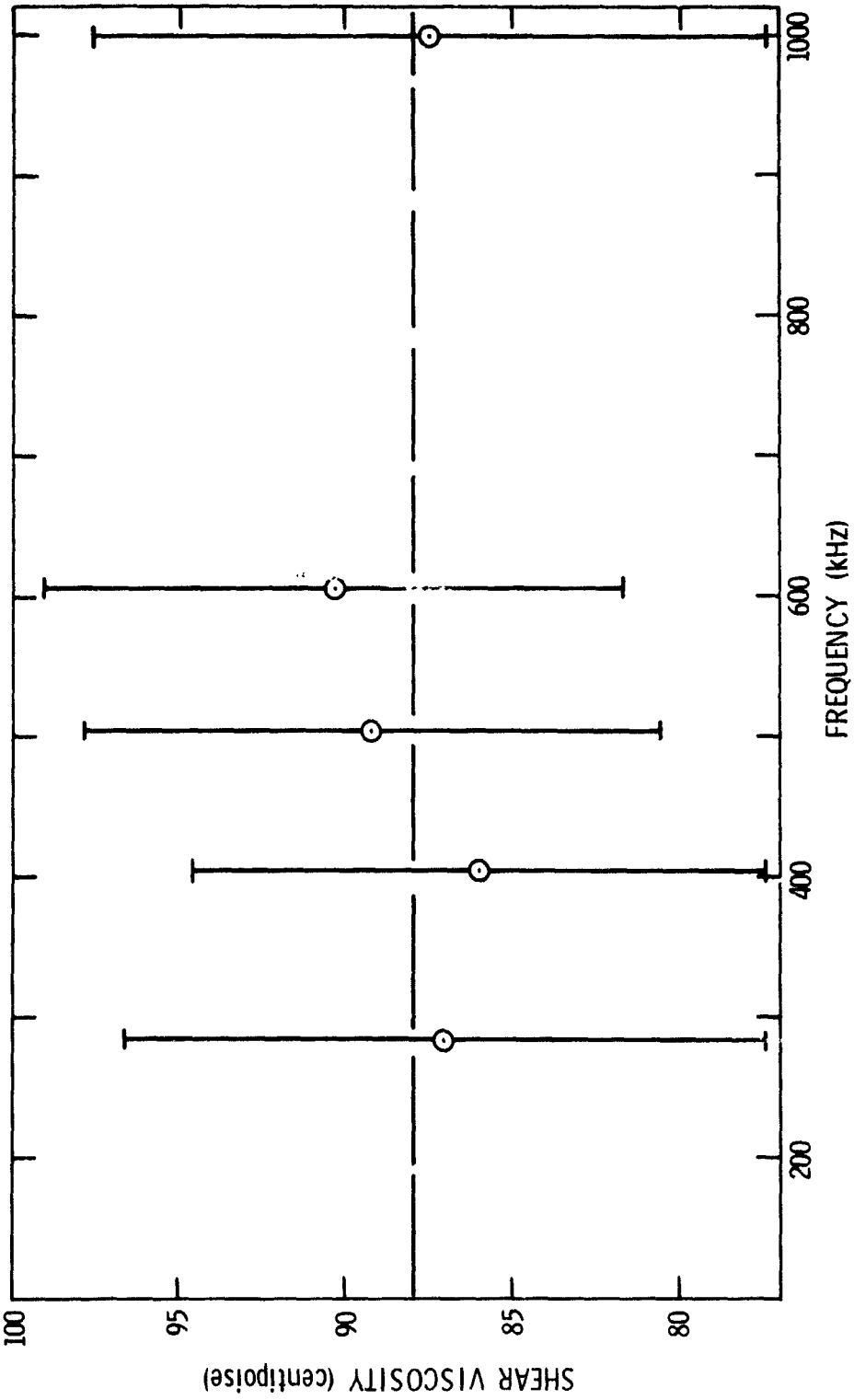

Figure 21. Shear viscosity of cedar wood oil, from 0.283 to 1.0 MHz.

Table III. Shear viscosity of water, NBS oils S-20 and S-600, varnish, and cedar wood as a function of frequency.

Liquid	Static viscosity (cp)	Shear viscosity(cp) for the following frequencies (kHz)						
		235	283	402	503	602	704	997
Water	0.89	0.55	0.85	0.50	1.40	0.79	0.65	0.44
S-20	38.7		39.1	36.9	41.0	41.6		38.3
S-600	1425		1484	1755	545	656	180	560
Varnish	60 ± 5	75.7	69.6	67.7	80.0	71.2		19.5
Cedar Wood	69 ± 5		87.0	86.0	89.2	90.3		87.5

4.2.4 Carbon Disulfide, Xylene, etc. Other liquids covering a wide range of viscosity were investigated at a single frequency and the results compared to the static viscosity. Table IV lists the results for liquids from carbon disulfide to xylene at 0.283 or 0.402 MHz. For most instances, the viscosity compared favorably to the static value.

4.3 Measurements of the Viscosity of Bonding Agents

Table V gives the viscosity for commonly used bonding agents ranging from caster oil to transducer-fluid 28. The table represents data at 0.283 and 0.402 MHz, and the dynamic viscosity is compared to the static values. Of all the liquids measured in this study, these bonding agents (with the exception of glycerin) had the least amount of scatter in the viscosity. The viscosity was less than the static values for all the agents measured.

4.4 Measurements of the Viscosity of Body Fluids

The viscosity of the body fluids of man and the domestic animals are largely unknown due to the small volumes of most fluids that are available for measurement. With this in mind, bile fluid and synovial fluid were withdrawn from bovines and fluid was extracted from the eye of a sheep (all three fluids were obtained from the Meat Laboratory at The Pennsylvania State University) and their viscosity measured at frequencies from 0.283 to 0.502 MHz.

Bile is a greenish, viscid fluid that is secreted by the liver to neutralize the hydrochloric acid from the stomach. The synovial fluid, as mentioned in Chapter I, lubricates the joints. The results

Table IV. Shear viscosity of numerous liquids.

Liquid	Static viscosity (cp)	Frequency (kHz)	Shear viscosity (cp)
Paint-thinner	3.2	283	2.5
Mineral oil	10.4	283	4.3
Carbon-disulfide	0.355	283	0.6
Nitro-benzene	2.03	283	0.8
Xylene	0.62	283	1.4
Detergent (Joy)	20.1	402	12.3

Table V. Shear viscosity of numerous bonding agents.

Liquid	Static viscosity (cp)	Frequency (kHz)	Shear viscosity (cp)
Glycerol	622.0	283	574.0
Caster oil	670.0	283	239.3
Dow Corning 200	35.0	402	8.8
Transducer fluid 28	100.0	402	73.4
Transducer fluid X	100.0 ± 5	402	71.3

for bile scattered greatly and may have been caused by sedimentation of its main constituents, producing changes in the viscosity. The viscosity of joint fluid was quite regular, as were the results for the eye fluid which was primarily made up of water.

The viscosity of uncoagulated whole blood taken from a finger prick was measured at two frequencies, and the results shown in Table VI. The results for the finger prick (consisting of whole blood containing fresh red cells, leukocytes and platelets, all suspended in plasma) were three times greater than the viscosities of red cells suspended in saline that had undergone metabolic changes during storage.

The data for all the body fluids measured are shown in Table VI. The results show that the shear viscometer is well applicable to the measurement of liquids of special interest to researchers in the medical fields.

4.5 Measurements of the Effect of Chemical Deformation of Red Blood Cells on the Viscosity of Blood

Blood cells are presently being studied by a number of investigators and by many different methods (16). The easy availability of bovine blood cells offered a unique opportunity for measuring the response of the viscometer to changes in the rheological properties of the red cells. Specifically, using bovine blood as a source of red cells, the deformability was changed by hematological methods and the viscosity measured.

4.5.1 Effect of Hematocrit on Viscosity. First, the effect of red cell volume (or hematocrit) on the viscosity was measured for two different suspensions. The suspensions were normal saline and normal

Table VI. Shear viscosity of four body fluids versus frequency.

	Shear viscosity (cp) at the following frequencies (kHz)		
Liquid	283	402	503
Bile	2.4	4.7	11.0
Eye	1.8	1.3	
Finger prick	15.4	16.5	
Joint fluid	2.0	1.8	1.5

saline with 20 mg/100 ml of sodium oleate added. As seen in Table VII, the 80% cell packing has a greater viscosity than the 40%, and this was true for both suspensions. Figure 22 shows this more clearly. As seen in Table VII, the shear viscosity was comparable to the measurements made with the Brookfield viscometer.

4.5.2 Effect of Sodium Oleate on Viscosity. Sodium oleate was used to change the shape of the red blood cells and the effect on the viscosity of a suspension containing these cells was measured with the shear and Brookfield viscometers (see Table VIII). The viscosity, measured with both instruments, increased when 20 mg/100 ml of sodium oleate was added to red cells suspended in normal saline. This may be seen in Figure 23.

4.5.3 Effect of Acetaldehyde on Viscosity. Acetaldehyde offers a method of changing red blood cell deformability without introducing geometric and internal viscosity changes. Therefore, acetaldehyde was added to bovine erythrocytes to stiffer their outer membrane, and the effect on viscosity was measured with both the shear and Brookfield viscometers. The addition of 1 ml/100 ml of acetaldehyde increased the viscosity as measured with both instruments (see Table IX). The results are also shown in Figure 24.

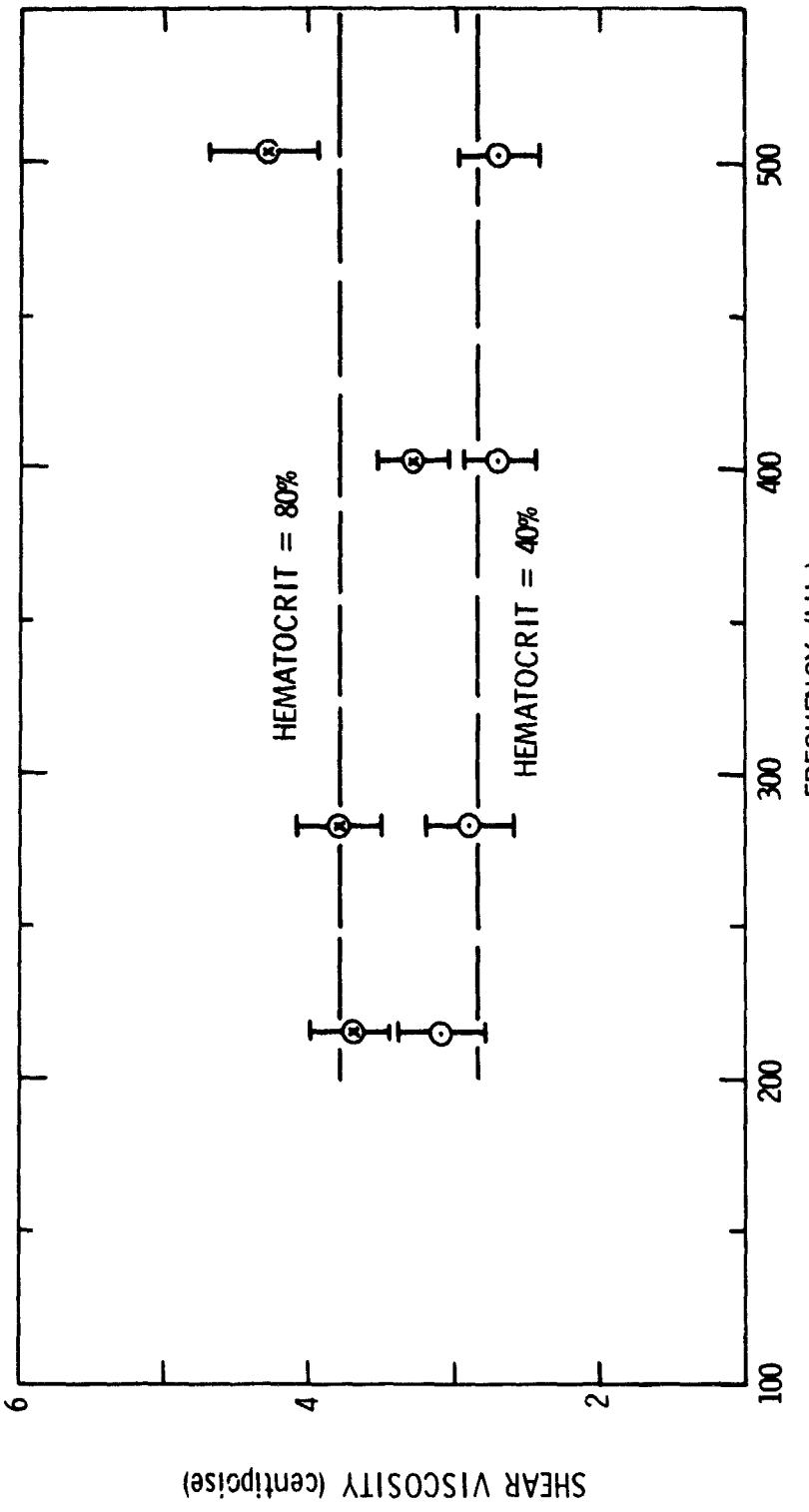

Figure 22. Shear viscosity of bovine erythrocytes in normal saline versus hematocrit.

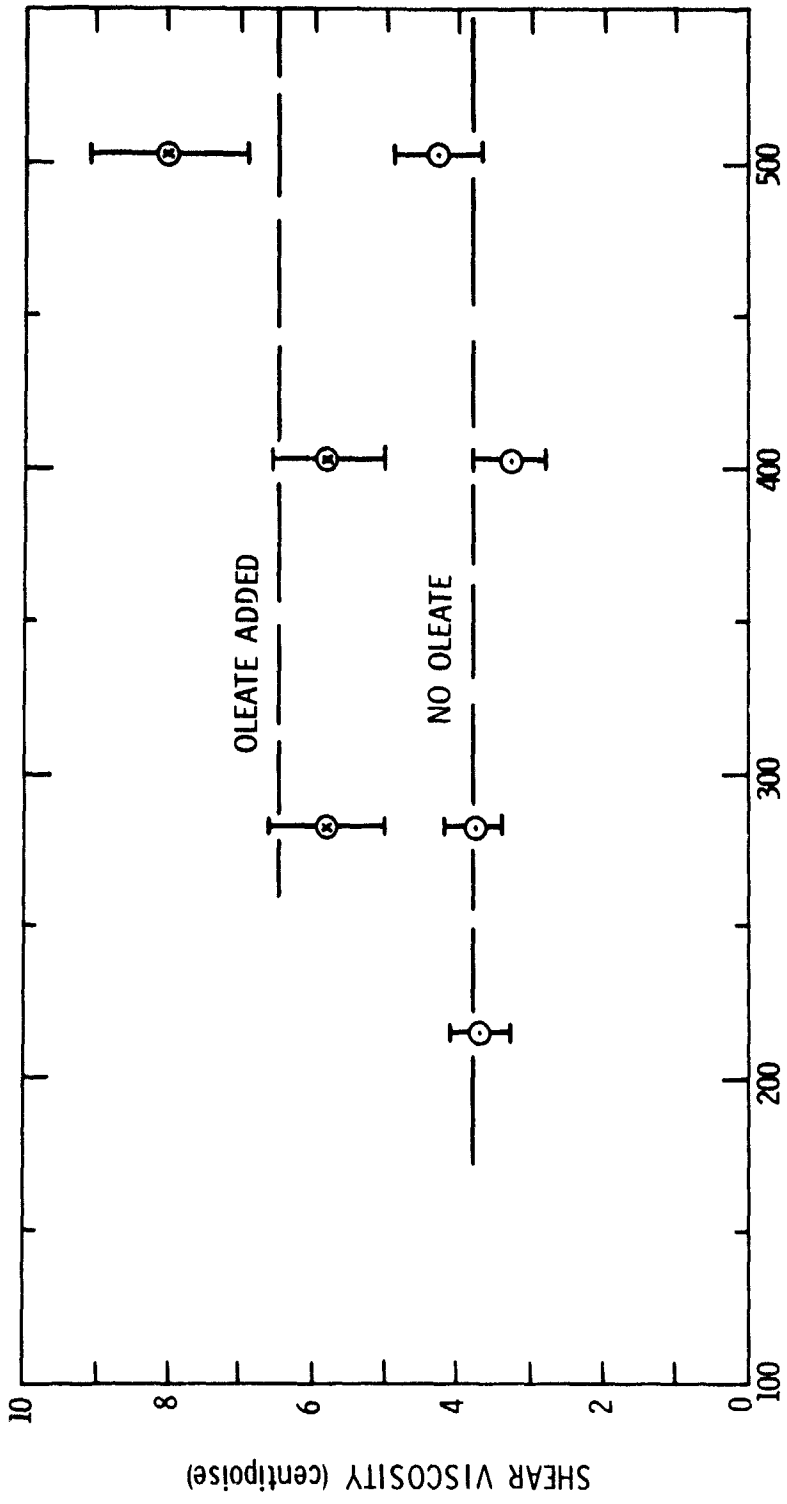

Figure 23. Shear viscosity of bovine erythrocytes in normal saline, with added 20mg/100 ml of sodium oleate.

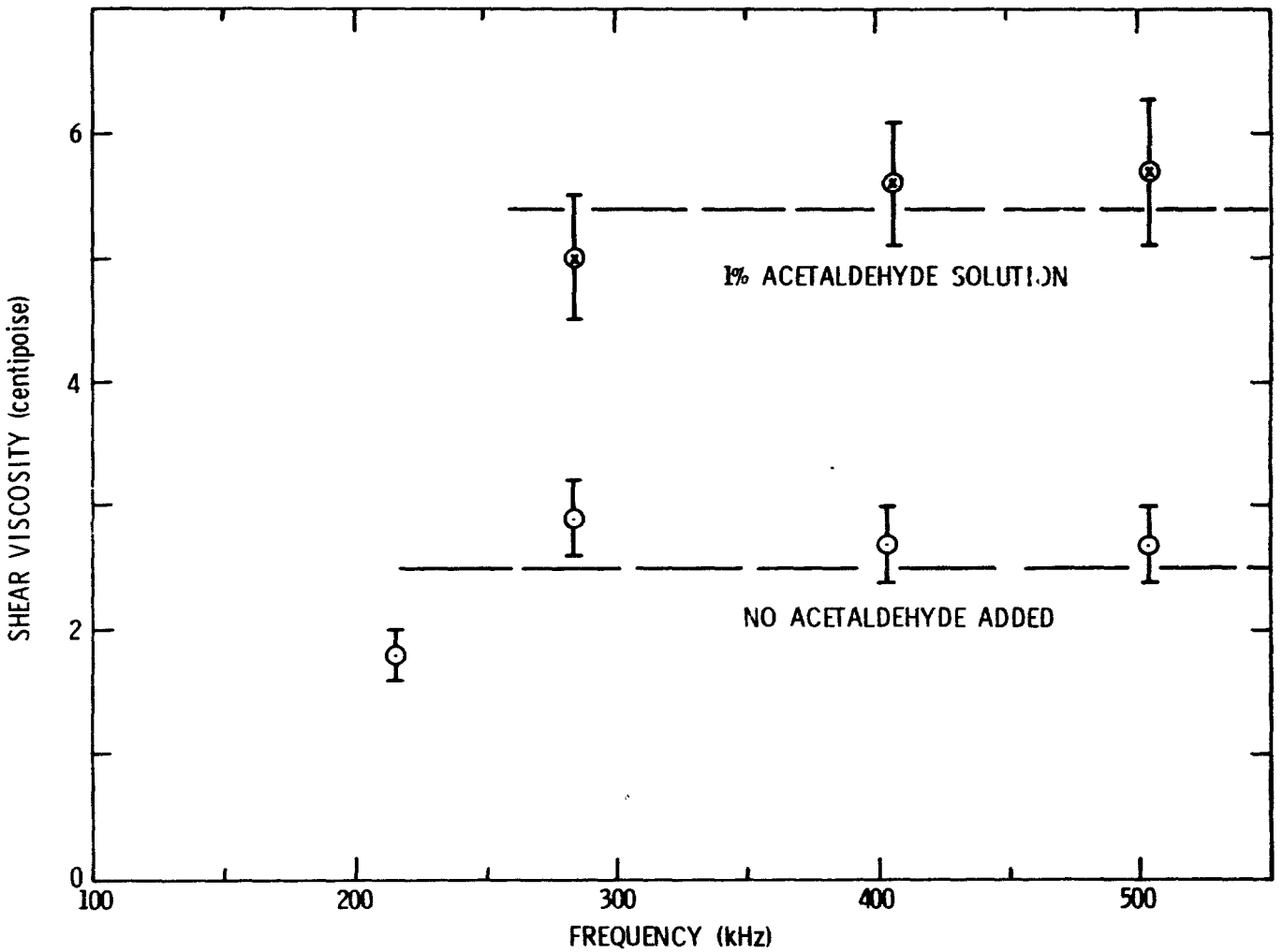

Figure 24. Shear viscosity of bovine erythrocytes in normal saline, with added 1ml/100 ml of acetaldehyde.

Table VII. Shear and Brookfield viscometric measurements with added 20 mg/100 ml of sodium oleate versus hematocrit.

		Shear viscometer			
		Shear viscosity measurements (cp) at the following frequencies in kHz			
Suspension	H(%)	215	283	402	503
Normal saline	40	3.1	2.9	2.7	2.7
Normal saline	80	3.7	3.8	3.3	4.3
Normal saline, with 20 mg/100 ml oleate	40	5.8	4.1	4.2	4.3
Normal saline, with 20 mg/100 ml oleate	80		5.8	5.8	8.0
		Brookfield viscometer			
		Viscosity measurements (cp) at the following strain rates in sec^{-1}			
		7.3	14.7	36.7	73.4
Normal saline	40	4.50	4.10	3.74	3.59

Table VIII. Shear and Brookfield viscometric measurements of bovine red cells resuspended in normal saline, with added 20 mg/100 ml of sodium oleate, at an elapsed time of four hours.

		Shear viscometer			
		Shear viscosity measurements (cp) at the following frequencies in kHz			
Suspension	H(%)	215	283	402	503
Normal saline	80	3.7	3.8	3.3	4.3
Normal saline, plus 20 mg/100 ml sodium oleate	80		5.8	5.8	8.0
		Brookfield viscometer			
		Viscosity measurements (cp) at the following strain rates in sec^{-1}			
		7.3	14.7	36.7	73.4
Normal saline	40	5.00	4.33	3.91	3.73
Normal saline, plus 20 mg/100 ml of sodium oleate	40	8.00	6.69	5.54	5.00

Table IX. Shear and Brookfield viscometric measurements for bovine erythrocytes resuspended in normal saline, with added 1 ml/100 ml of acetaldehyde.

		Shear viscometer			
		Shear viscosity measurements (cp) at the following frequencies in kHz			
Suspension	H(%)	215	283	402	503
Normal saline	40	1.8	2.9	2.7	2.7
Normal saline, plus 1% acetaldehyde	53		5.0	5.6	5.7
		Brookfield viscometer			
		Viscosity measurements (cp) at the following strain rates in sec^{-1}			
		7.3	14.7	36.7	73.4
Normal saline	40	4.70	4.38	3.96	3.83
Normal saline, plus 1% acetaldehyde	47	6.00	5.65	5.66	5.90

CHAPTER V

SUMMARY AND CONCLUSION

5.1 Summary

The problem of this investigation was to develop an inexpensive, precision viscometer capable of measuring small liquid volumes, such as drops. The approach was to utilize the short effective path length of shear waves in liquids. The viscometer consists of an unplated crystal bar excited by a 50 ms pulse, and suitable electronics to observe and record the decaying vibrations after the power is shut off. There are two measured time constants t_e defined as the time it takes for the waveform to reach 1/e of its initial amplitude. The first decay time t_e^0 is for the crystal driven in air. The second decay time is measured when the crystal decays with a liquid on its surface. The difference between these decay times is a measure of the effect of the liquid and gives the system loss factor.

We consider the case, through proper experimental arrangement, where the greatest loss is the shear energy loss in the liquid. All other losses are negligible, including the crystal mounting loss.

A crystal orientation analysis was made to insure a dominant thickness-shear mode. After the proper crystal cut was selected, a dimensional analysis was necessary to reduce coupling between the shear and flexure modes.

There was no reason to believe that the crystal surface vibrates with a uniform velocity. The surface velocity distribution was found by placing drops of glycerin at various positions on the working

surface. The velocity was a maximum at the center and decreased towards the boundaries of the plate. The crystal mode mass was determined from these measurements to be $\frac{1}{2\sqrt{2}} M^Q$, where M^Q is the crystal static mass.

Extensive measurements were made of the viscosity as a function of liquid contact area, since the energy losses were influenced by the liquid configuration. Peaks in the shear viscosity were due to compressional resonances that generate a relative motion parallel to the surface of the crystal. These peaks were ignored. The lower parts of the viscosity curves were averaged and the average constituted the measured viscosity at that frequency.

The shear viscometer was applied to a variety of liquids ranging from benzene to xylene. The measurements for a droplet of water were close to the static value of 0.89 cp for all values from 100 to 1000 kHz, except between 400 to 500 kHz where the viscosity increased. The increase in droplet viscosity was greater than the uncertainty of the measurement and was not due to the molecular properties of water where a relaxation phenomenon would decrease with frequency. It is likely that the increase was due to surface tension, which produced a scattering in the data of all the liquids measured in this study. Unfortunately, the method of measuring the effect of surface tension (by placing drops on top of each other, thereby increasing the radius of curvature while keeping the surface contact area fixed) was not sensitive enough to isolate surface tension in the presence of compressional droplet resonances.

A National Bureau of Standards oil S-600, was measured from 283 to 1000 kHz. The low frequency results were near the static value of 1425 cp. However, beginning at 402 kHz, the viscosity decreased dramatically. This decrease could have been due to molecular relaxation which is possible at these high frequencies for high viscosity oils.

The Satin XL-8 Urethane Varnish viscosity value at 996 kHz of 19.5 cp was also well below the static value of 60 ± 5 cp. The decrease could be due to the absorption of energy in the long molecular chains of the polymer base.

A few commonly used acoustic bonding agents were examined, ranging from Castor Oil to Dow-Corning 200. The data for these bonding agents was the most repeatable of all the liquids examined in this study.

The shear viscometer provided a new tool for examining liquids of special interest to researchers in the medical fields. Knowledge of the body fluids of man is meager, largely due to the small volumes available for measurement. For instance, the viscosity of joint fluid was measured and the result varied from 1.5 to 2.0 cp. The results for uncoagulated whole blood from a finger prick were three times greater than blood that had undergone metabolic changes during storage.

The applicability of the shear viscometer to medical research was examined by investigating the response of the viscometer to rheological changes of bovine red blood cells. Specifically, the deformability of red cells was regulated by standard hematological methods using sodium oleate, acetaldehyde and hematocrit, and the viscosity measured with the high frequency shear viscometer and the low strain rate Brookfield viscometer. Sodium Oleate changed the shape of the red cells and

acetaldehyde stiffened the outer membrane. The results show that the dynamic viscosity increases with the addition of sodium oleate, acetaldehyde, or hematocrit. The Brookfield data was comparable.

5.2 Conclusion

Internal friction is a consequence of molecular and atomic relaxation phenomenon. For fluids, only a limited number of discrete relaxations are superimposed on each other. The viscosity is constant at low frequencies as long as the sound period is larger than the relaxation time constant; at higher frequencies, the viscosity decreases with the frequency. We would, therefore, always expect the viscosity to be a maximum for static flow and other low frequency measurements and decrease only at the higher frequencies. Therefore, a peak in the viscosity curve indicates an unusual behaviour of the fluid. Such peaks have been observed in this study.

Most measurements in this study lead to a value of viscosity not very different from the static viscosity, and some (see the data for NBS S-600 oil) indicate clearly a simple relaxation. However, there are some instances where the high frequency drop viscosity turns out to be greater than the static value (see water, for instance). This could be a surface tension effect. It is still unclear how this effect is coupled with the sound motion and with the radius of curvature of the drop. It is possible that the method used to increase the volume (keeping surface contact area constant) is not sensitive enough to isolate surface tension effects. It has also been suggested that, since the measurements were made at room conditions, the liquid layer near the drop surface accumulates impurities and can consequently

prevent the crystal from being in perfect contact with the liquid. Special tests could be designed to test whether impurities effect the measurements.

The variations in the viscosity were greater than were expected, and detailed studies will be required to clarify the effect of surface tension. However, the goal of this thesis to produce a useful method of investigating drops of fluids has been fully attained. The method is very simple and practical, and the results are reproducible.

BIBLIOGRAPHY

1. A. J. Matheson, Molecular Acoustics (New York: Wiley-Interscience, 1973).

2. W. L. Ghering, "Ultrasonic Coupling Losses," Ph.D. Thesis, The Pennsylvania State University, 1968.

3. R. N. Hosier, "Ultrasonic Viscosity Measurements," M.S. Thesis, The Pennsylvania State University, 1969.

4. R. N. Hosier, "Ultrasonic Viscosity Measurements," M.S. Thesis, The Pennsylvania State University, 1969, p. 44.

5. H. Schmid-Schonbein and R. E. Wells, "Fluid Drop-Like Transitions of Erythrocytes Under Shear," Science 165, 288-291 (1969).

6. H. Ekstein, "Forced Vibrations of Piezoelectric Crystals," Phys. Rev. 70, 76-84 (1946).

7. E. Skudrzyk, Simple and Complex Vibratory Systems (The Pennsylvania State University Press, University Park, Pa., 1968).

8. E. Skudrzyk, Simple and Complex Vibratory Systems (The Pennsylvania State University Press, University Park, Pa., 1968) p. 64.

9. E Skudrzyk, Simple and Complex Vibratory Systems (The Pennsylvania State University Press, University Park, Pa , 1968) p. 65.

10. S. Chien, "Biophysical Behavior of Red Cells in Suspensions," The Red Blood Cell (New York: Academic Press, 1975) pp 1031-1133.

11. M. Belzar, "The Effect of Erythrocyte Deformability Upon the Viscosity and Stability of Bovine Red Cell Suspensions in Circular Couette Flow," M.S. Thesis, The Pennsylvania State University, 1976

12. R. N. Hosier, "Ultrasonic Viscosity Measurements," M.S. Thesis, The Pennsylvania State University, 1969, p 18

13. R A Sykes, Bell System Techn J 23, 52 (1944).

14 R. N. Hosier, "Ultrasonic Viscosity Measurements," M.S Thesis, The Pennsylvania State University, 1969, p 39.

15 A. Klemm, "Kataphorese von Gasblasen," Physikolische Zeitschrift 39. 783 (1938). "Die Dampfung von Kapillarwellen," Physikolische Zeitschrift 40, 483 (1939).

16 S. Chien, "Biophysical Behavior of Red Cells in Suspensions," The Red Blood Cell (New York: Academic Press, 1975) pp 1031-1133.

17. W. P. Mason, Piezoelectric Crystals and their Applications to Ultrasonics (New York: Van Nostrand Co., 1950).

18. R. A. Sykes, "Modes of Motion in Quartz Crystals, the Effects of Coupling, and Methods of Design," Quartz Crystals and Electrical Circuits, ed. R. H. Heising, Chapter 6 (New York: Van Nostrand Co., 1946).

19. R. A. Sykes, "Modes of Motion in Quartz Crystals, the Effects of Coupling, and Methods of Design," Quartz Crystals and Electrical Circuits, ed. R. H. Heising, Chapter 6 (New York: Van Nostrand Co., 1946) 237.

APPENDIX A

CRYSTALLOGRAPHIC ANALYSIS OF THE CRYSTAL VIBRATOR

The following considerations prove the advantages of the AT quartz crystal cut over the normally used Y-cut.

An infinite quartz crystal has many modes of motion: flexural, face-shear, dilatational, and thickness-shear. The latter three types of motion are coupled by mutual elastic coefficients s_{ij} whose value has to be reduced to eliminate these troublesome modes. Consider a special infinite quartz plate known as a Y plate, cut such that the larger face contains the XZ plane and has the Y axis for a surface normal. The total strain induced is the sum of the mechanical strain $s_{ij}T_j$ and the electrical strain $d_{mj}E_j$, where the stress-strain relations exhibit trigonal symmetry. The total electric displacement is the sum of the polarization $e_{ni}S_n$ and $\varepsilon_{mn}E_n$. The sum of the two relations are

$$S_1 = s_{11}T_1 + s_{12}T_2 + s_{13}T_3 + s_{14}T_4 + d_{11}E_1 \quad ,$$

$$S_2 = s_{12}T_1 + s_{11}T_2 + s_{13}T_3 - s_{14}T_4 - d_{11}E_1 \quad ,$$

$$S_3 = s_{13}T_1 + s_{13}T_2 + s_{33}T_3 \quad ,$$

$$S_4 = s_{14}T_1 - s_{14}T_2 + s_{44}T_4 + d_{14}E_1 \quad ,$$

$$S_5 = s_{44}T_5 + 2s_{14}T_6 - d_{14}E_2 \quad ,$$

$$S_6 = 2s_{14}T_5 + 2(s_{11}-s_{12})T_6 - 2d_{11}E_2 \quad ,$$

$$D_1 = e_{11}S_1 - e_{11}S_2 + e_{14}S_4 + \varepsilon_{11}E_1 \quad ,$$

$$D_2 = -e_{14}S_5 - e_{11}S_6 + \varepsilon_{11}E_2 \quad ,$$

and $$D_3 = \varepsilon_{33}E_3 \quad , \qquad \text{(A 1)}$$

where S_1, S_2, S_3 are the longitudinal strains and S_4, S_5, S_6 the shear strains. The compliance coefficients s_{16} (i = 1,2,...5) couple other modes to the thickness shear motion. Of special importance are the coefficients s_{16} and s_{26} that couple dilatational modes to shear. In Y-cut crystals, $s_{16} = s_{26} = 0$ and dilatational motion should not exist.

Consider our case where an electric field E_2 is the initial source of strain. Only if E_2 exists in a particular row in Equation (A.1) will the strain of that row survive. Equation (A.1) becomes

$$S_5 = s_{44}T_5 + 2s_{14}T_6 - d_{14}E_2$$

$$S_6 = 2s_{14}T_5 + 2(s_{11}-s_{12})T_6 - 2d_{11}E_2 \qquad \text{(A.2)}$$

and

$$D_2 = -e_{14}S_5 - e_{11}S_6 + \varepsilon_{11}E_2 \ ,$$

where the strains are referred to the strained coordinates ψ_i by

$$S_5 = \frac{\partial \psi_1}{\partial x_3} + \frac{\partial \psi_3}{\partial x_1} \qquad \text{(face-shear)}$$

and (A.3)

$$S_6 = \frac{\partial \psi_2}{\partial x_1} + \frac{\partial \psi_1}{\partial x_2} \qquad \text{(thickness-shear)} \ .$$

The electric field E_2 therefore produces two strains, S_5, S_6. The S_5 strain (face-shear) distorts the crystal in the xz plane. The S_6 (thickness-shear) distorts the crystal in the xy plane. Rewriting Equation (A.2) in terms of the strains, the electric coefficients c_{ij} and the piezoelectric constants e_{ij}.

$$T_5 = c_{55}S_5 + c_{56}S_6 + e_{14}E_2$$

$$T_6 = c_{56}S_5 + c_{66}S_6 + e_{11}E_2 \qquad \text{(A 4)}$$

and

$$D_2 = -e_{14}S_5 - e_{11}S_6 + \varepsilon_{11}E_2 \ .$$

Equation (A.4) is the important coupling equation between face-shear and thickness shear The strain S_6 produces the S_5 strain, the elastic constant c_{56} being a measure of the coupling.

One method of reducing the coupling is to decrease, by a change in the orientation, the magnitude of c_{56}. The value of c_{56} depends on the rotation of the crystal cut about the x axis (that is, the angle θ between the z and the rotated z axis). The cut of $\theta = 31°$ has been called the Y cut. The cut of $\theta = 35°$, known as the AT cut, has the low value of $c'_{56} = 60 \times 10^{-10}$ c.g.s., a zero temperature coefficient and a relatively active electric modulus d_{14} connecting E_2 to the S_6 strain (17). The elimination from temperature influence is especially important when using shear waves. Crystals from the AT family were chosen for this study, since these crystals have fewer subsidiary resonances.

The AT-cut plate also gives a maximum of energy output from the crystal face. The place is cut such that the transverse vibration has its motion in a direction of sub-minimum elastic modulus, giving a maximum amplitude of vibration.

APPENDIX B

DIMENSIONAL ANALYSIS OF THE AT-QUARTZ PLATE

When dealing with plates of finite dimensions, flexure and face shear arise from the presence of the crystal boundaries. The higher order harmonics of flexure are especially troublesome, since their equation of motion is identical to thickness shear.

It becomes necessary to select dimensions of the crystal in such a manner that the three types of modes have different frequencies and their harmonics do not intersect. The motion of a crystal is entirely determined by the dimensions of the plate. The coupling of the unwanted modes can therefore be avoided by choosing the proper length and width such that the unwanted modes do not intersect the experimental thickness-shear frequency curve in the region of interest. For instance, the regular pattern of coupling between flexure and thickness-shear is expressed by the experimental formula (18).

$$f_{x_f} = \frac{1338.4}{x(\text{mm})} n_{x_f} \text{ kHz} , \qquad (B.1)$$

where x is the length of the crystal and n_{x_f} is the order of flexure for n = 1,2,... .

The coupling to harmonics of low frequency face shear depends on both the length and the width dimensions. Again, experimental evidence is used. The frequency of coincidence of face shear and thickness-shear in AT plates is expressed by two separate formulas (19),

$$f_{x_s} = \frac{254.2}{x(cm)} n_{x_s} \text{ kHz}$$

and (B.2)

$$f_{z_s} = \frac{254.0}{z'(cm)} n_{z_s} \text{ kHz}$$

where x = length of the crystal,

z' = width of the rotated crystal,

n_{x_s} = order of face shear along x, and

n_{z_s} = order of face shear along z'.

Crystal dimensions were predetermined so that integer flexure and face shear were not present. Table X is a list of the crystals bought from Valpey Fisher, covering the range from 100 kHz to 5 MHz. None of the crystals have an integer flexure order. Crystal #7 does have a high order face shear (#13) motion. However, this order is too high to be troublesome.

Table X. Flexure and face-shear modes of quartz crystals

Crystal(#)	F(kHz)	M(gms)	Length x(mm)	Width z(mm)	Thickness y(mm)	n_{x_f}	n_{x_s}	n_{z_s}
1	106.5	21.920	45	11	17	3.5	1.9	0.46
2	215.0	10.060	45	11	8	7.2	3.8	0.93
3	283.8	7.852	45	11	6	9.5	5.3	1.23
4	402.1	5.45	45	11	4	13.5	7.2	1.74
5	502.9	4.35	45	11	3	16.9	8.9	2.18
6	2000.0	1.16	45	11	0.9	67.2	35.2	8.7
7	3000.0	0.778	45	11	0.6	100.9	53.2	13.0
8	4000.8	0.584	45	11	0.45	134.5	70.8	17.3
9	5000.5	0.467	45	11	0.4	168.1	88.5	21.7

APPENDIX C

DETERMINATION OF THE CORRECTION FACTOR

Define the system loss factor due to sound radiation to be

$$\Delta\eta = \frac{1}{\omega}\frac{\text{Energy Loss due to Radiation}}{\text{Total Energy of the System}}$$

$$= \frac{1}{\omega}\frac{\frac{1}{2}\sigma_Q\rho_0 c_0 V_{dil}^2}{\frac{1}{2}M_v^Q(V_{sh}^2+V_{dil}^2)}, \tag{C.1}$$

where σ_Q = surface area of the vibrator,

$\rho_0 c_0$ = characteristic impedance of vibrator in air, and

V_{dil} = maximum dilatational velocity.

Approximating the mean velocity amplitude by $\frac{1}{\sqrt{2}} V_{dil}$, the loss factor becomes

$$\Delta\eta = \frac{1}{\omega}\frac{\sigma_Q\rho_0 c_0}{\frac{1}{2}M^Q(1+\frac{1}{\Delta^2})} . \tag{C.2}$$

Since

$$M^Q = \rho_Q c_Q h$$

$$= \rho_Q c_Q \frac{\lambda}{2} , \tag{C.3}$$

where

$$\rho_0 c_0 = 42 \text{ gm/sec-cm}^2$$

$$\rho_Q c_Q = 1.51 \times 10^6 \text{ gm/sec-cm}^2 , \tag{C.4}$$

therefore,

$$1 + \frac{1}{\Delta^2} = \frac{17.7 \times 10^{-6}}{\Delta\eta} .$$

VITA

Edward Shalis was born in Mariepol, Ukraine (U.S.S.R.). He graduated from Central High School, in Philadelphia, Pennsylvania in 1959. The author attended Temple University (B.A. Physics, 1963), Penn State University (M.S. Physics, 1968), and Cornell University (1968-1969). He resumed full time study for his doctorate at Penn State in 1971.

The author wishes to dedicate this dissertation to the memory of his parents, Olga (1915-1968) and Wolodymer (1913-1971).

DISTRIBUTION LIST

Commander (NSEA 09G32)
Naval Sea Systems Command
Department of the Navy
Washington, D. C. 20362 — Copies 1 and 2

Commander (NSEA 0342)
Naval Sea Systems Command
Department of the Navy
Washington, D. C. 20362 — Copies 3 and 4

Defense Documentation Center
5010 Duke Street
Cameron Station
Alexandria, VA 22314 — Copies 5 through 16